ICP/EXT-04-00321
Revision 0

Near-Field Simulation of Carbon-14 and Tritium Migration from Buried Beryllium Blocks in the Subsurface Disposal Area

Gopi Nalla

Idaho Completion Project

Bechtel BWXT Idaho, LLC

August 2004

ICP/EXT-04-00321
Revision 0
Project No. 23378

Near-Field Simulation of Carbon-14 and Tritium Migration from Buried Beryllium Blocks in the Subsurface Disposal Area

Gopi Nalla

August 2004

Idaho Completion Project
Idaho Falls, Idaho 83415

Prepared for the
U.S. Department of Energy
Assistant Secretary for Environmental Management
Under DOE Idaho Operations Office
Contract DE-AC07-99ID13727

ABSTRACT

This report describes a computer simulation of the near-field release, fate, and transport of tritium and carbon-14 from the buried beryllium blocks in Soil Vault Row 20 in the Subsurface Disposal Area. The Subsurface Disposal Area is a radioactive waste landfill in the Radioactive Waste Management Complex, part of the Idaho National Engineering and Environmental Laboratory. The study uses TETRAD, a multiphase, multicomponent, three-dimensional simulator. This report describes the numerical model's governing equations of flow and transport of tritium and carbon-14, implementation, calibration and prediction of diffusional migration into the atmosphere, and transport into the vadose zone in the near field of the buried beryllium blocks in Soil Vault Row 20.

This work supports Operable Unit 7-13/14 by simulating the near-field diffusional migration of $^{14}CO_2$ into the atmosphere that is not captured by the overall model, whose smallest horizontal dimension is 38.1 m on a side. The overall model simulates the possibility of $^{14}CO_2$ migration further into the vadose zone and the Snake River Plain Aquifer.

EXECUTIVE SUMMARY

A numerical model was developed to investigate the near-field release, fate, and transport of tritium and carbon-14 from the buried beryllium blocks in Soil Vault Row 20 in the Subsurface Disposal Area. The Subsurface Disposal Area is a radioactive waste landfill in the Radioactive Waste Management Complex, part of the Idaho National Engineering and Environmental Laboratory. The study uses TETRAD, a multiphase, multicomponent, three-dimensional simulator. This report describes the numerical model's governing equations of flow and transport of tritium and carbon-14, implementation, calibration and prediction of diffusional migration into the atmosphere, and transport into the vadose zone in the near field of the buried beryllium blocks in Soil Vault Row 20.

To estimate the migration of $^{14}CO_2$, a near-field model is necessary because the present overall model's smallest horizontal unit is 38.1 m/side. The overall model with this unit size is capable of simulating the entire vadose zone and the Snake River Plain Aquifer, but a model capable of near-field simulation is required to capture the diffusional migration of $^{14}CO_2$ from the high-concentration gradients in the vicinity of the beryllium blocks, the source of this contamination. To capture this information, TETRAD—a multiphase, multicomponent simulator—was used to implement one-dimensional and two-dimensional, cylindrical coordinate, numerical models. This application of the model was validated with contaminant concentrations monitored at several locations laterally in the soil column and estimated diffusion rates to the atmosphere based on concentration measurements above the disposal location. The numerical model provides a tool to predict the tritiated water and $^{14}CO_2$ concentrations in the vadose zone, the diffusion rates of these contaminants into the atmosphere, and the effective source release rates retained in the subsurface.

The one-dimensional model accounts for only the vertical transport of contaminants, while the two-dimensional model accounts for both the vertical and the lateral migration of contaminants. Assumptions of homogenous sedimentary soil layers and isothermal conditions were used in both one-dimensional and two-dimensional models. Sensitivity analysis performed on the one-dimensional model showed that the infiltration rate had a major effect, while the barometric pumping, relative permeability, and residual water saturation had insignificant effects on the tritiated water surface diffusion rate to the atmosphere.

The two-dimensional radial model is more accurate than the one-dimensional model; it allows lateral migration and also was calibrated with monitoring data from measurement ports in the soil layers. The two-dimensional model concludes that, over a 22-year simulation period, the cumulative surface diffusional migration of $^{14}CO_2$ to the atmosphere accounts for 82% of the cumulative source released, while the cumulative surface diffusional migration of tritiated water accounts for 0.6% of the cumulative source released. These results suggest that a major fraction of the released $^{14}CO_2$ is lost to the atmosphere by surface diffusion, while a major fraction of tritiated water is retained in the subsurface.

The overall conclusion is that the carbon-14 release rates from the beryllium blocks for the Operable Unit 7-13/14 full vadose zone model should be scaled down by a time-variant factor to account for near-field diffusional migration to the atmosphere.

ACKNOWLEDGMENTS

The authors would like to thank the U.S. Department of Energy Idaho Operations Office for funding the project. We would like to thank Paul D. Ritter for providing the data on measurements taken during the performance assessment/composite assessment and in the conceptual model construction. We also express our thanks to Art D. Rood for helping us in understanding his one-dimensional model of Soil Vault Row 20 and for providing a basis to start this modeling project, and to Pete Martian for his informative discussions and engineering design file on the transport and hydrogeologic parameters. We also would like to thank George M. Shook for making the TETRAD simulator available for environmental applications and Jeffrey A. Sondrup for debugging the model.

CONTENTS

FIGURES

TABLES

Near-Field Simulation of Carbon-14 and Tritium Migration from Buried Beryllium Blocks in the Subsurface Disposal Area

1. INTRODUCTION

This report describes the development, validation, and results of a computer model created to estimate the migration of $^{14}CO_2$ in the near field, or vicinity, of beryllium reflector blocks buried in the Subsurface Disposal Area (SDA), a radioactive landfill in the Radioactive Waste Management Complex, located in the Idaho National Engineering and Environmental Laboratory (INEEL). The results of this simulation support the overall modeling effort for Waste Area Group (WAG) 7 Operable Unit (OU) 7-13/14. The present overall model's smallest horizontal unit is 38.1 m/side. It is capable of modeling the entire vadose zone and the Snake River Plain Aquifer, but a model capable of near-field modeling is necessary to capture the diffusional migration of $^{14}CO_2$ caused by the large concentration gradients in the near field of the beryllium blocks, the source of this contamination. To capture this information, TETRAD—a multiphase, multicomponent code—was used to develop a numerical model that is two-dimensional and has cylindrical coordinates. This new numerical model was validated with the contaminant concentrations monitored at several locations laterally in the soil column and above an actual disposal location. The numerical model provides a tool to predict the tritiated water (HTO) and $^{14}CO_2$ concentrations in the vadose zone, the diffusional migration rates of these contaminants into the atmosphere, and the effective source release rates retained in the subsurface.

Based on data from this near-field model, the report concludes that cumulative surface diffusional migration of $^{14}CO_2$ to the atmosphere accounts for 80% of the cumulative released source over a 22-year simulation period. Estimates of the amount of $^{14}CO_2$ that remains in the subsurface, therefore, should be scaled down to account for diffusional migration to the atmosphere.

1.1 Purpose

Results from this simulation support the overall modeling effort and a better understanding of possible migration of $^{14}CO_2$ for the remedial investigation/feasibility study (RI/FS) for OU 7-13/14.[a] The plan describing requirements for the RI/FS is in the *Second Revision to the Scope of Work for the Operable Unit 7-13/14 Waste Area Group 7 Comprehensive Remedial Investigation/Feasibility Study* (Holdren and Broomfield 2003).

1.2 Overview

Field-monitoring data and modeling of contaminant fate and transport suggest that carbon-14 (^{14}C) is a contaminant of concern (Holdren and Broomfield 2003). One of the primary waste streams containing ^{14}C is the beryllium reflector blocks that were used as neutron reflectors in nuclear test reactors at the INEEL. Soil Vault Row 20 (SVR-20) contains buried beryllium blocks that have been monitored since 1996. When released through corrosion of the beryllium blocks, tritium (^{3}H) and ^{14}C form the compounds HTO and $^{14}CO_2$ that are mobile in both the liquid and gaseous phases of the vadose zone. A numerical model is necessary to simulate the near-field migration of ^{14}C and ^{3}H and identify amounts of

a. The *Federal Facility Agreement and Consent Ord*er (DOE-ID 1991) lists 10 WAGs for the INEEL. Each WAG is subdivided into OUs. The RWMC is identified as WAG 7 and originally contained 14 OUs. Operable Unit 7-13 (transuranic pits and trenches RI/FS) and OU 7-14 (WAG 7 comprehensive RI/FS) were ultimately combined into the OU 7-13/14 comprehensive RI/FS for WAG 7.

contaminants released from the beryllium blocks, the expected concentrations at near-source locations, and amounts of contaminants released to the atmosphere. The near-field model results provide an effective source term for the entire vadose zone model and, therefore, affect evaluation of possible migration in the groundwater pathway.

1.3 Scope

This report documents development and validation of the near-field model, results of the model, and a recommendation for using these results.

The physical scope of the modeling effort is focused on the near-source environment. The specific modeling objectives are to:

- Develop a one-dimensional (1-D) and two-dimensional (2-D), multiphase coupled flow and transport model to simulate the release and transport of HTO and $^{14}CO_2$ from the buried irradiated beryllium blocks into the near-source subsurface
- Calibrate the models to monitoring data (i.e., concentrations of HTO and $^{14}CO_2$ in the vadose zone and rates of migration of HTO into the atmosphere)
- Determine the sensitivity of the simulated transport of contaminants to model parameters
- Predict the diffusional migration rates of $^{14}CO_2$ into the atmosphere, thus providing an effective source term for the vadose zone portion of the groundwater pathway evaluation.

1.4 Brief History and Description of the Idaho National Engineering and Environmental Laboratory

The INEEL, originally established in 1949 as the National Reactor Testing Station, is a DOE-managed reservation that historically has been devoted to energy research and related activities (see Figure 1). The SDA is part of the Radioactive Waste Management Complex, a group of contiguous waste management facilities and support areas covering 71.6 ha (177 acres) in the southwestern quadrant of the INEEL. In 1952, the SDA was established at 5.26 ha (13 acres) for disposal of solid radioactive waste. Burial of defense waste with transuranic elements from the Rocky Flats Plant began in 1954; by 1957, the original SDA was nearly full. In 1958, the SDA was expanded to 35.6 ha (88 acres), which remained the same until 1988 when the security fence was relocated outside the dike surrounding the SDA, and the current size of 39.3 ha (97 acres) was established. Radioactive waste was buried in pits, trenches, and soil vault rows excavated into a veneer of surficial sediment (see Figure 2 for a map of the Radioactive Waste Management Complex showing the location of the SDA). Contaminants in the SDA radioactive waste landfill include materials produced during manufacture of weapons at the Rocky Flats Plant, fission and activation products resulting from on- and off-INEEL reactor operations, and hazardous chemicals associated with all waste sources.

Most of the irradiated beryllium waste in the SDA came from the Advanced Test Reactor (ATR), Engineering Test Reactor, and Materials Test Reactor, which are located at the Test Reactor Area. Activated beryllium reflectors and other irradiated components were buried in pits and soil vaults in the SDA between 1970 and 1993. The beryllium had been used as a neutron reflector in these nuclear test reactors. The buried waste includes 20 beryllium blocks from ATR Cores 1, 2, and 3; nine outer shim control cylinders from ATR Cores 1 and 2; and one beryllium reflector assembly each from the Materials Test Reactor and Engineering Test Reactor. Results of monitoring from functioning probes at the SVR-20

beryllium burial location indicate that specific activity of ^{14}C in samples is approximately two to five orders of magnitude above the typical background concentration of ^{14}C, which is 6.5 pCi/g of total carbon (Olson et al. 2003; Koeppen et al. 2004).

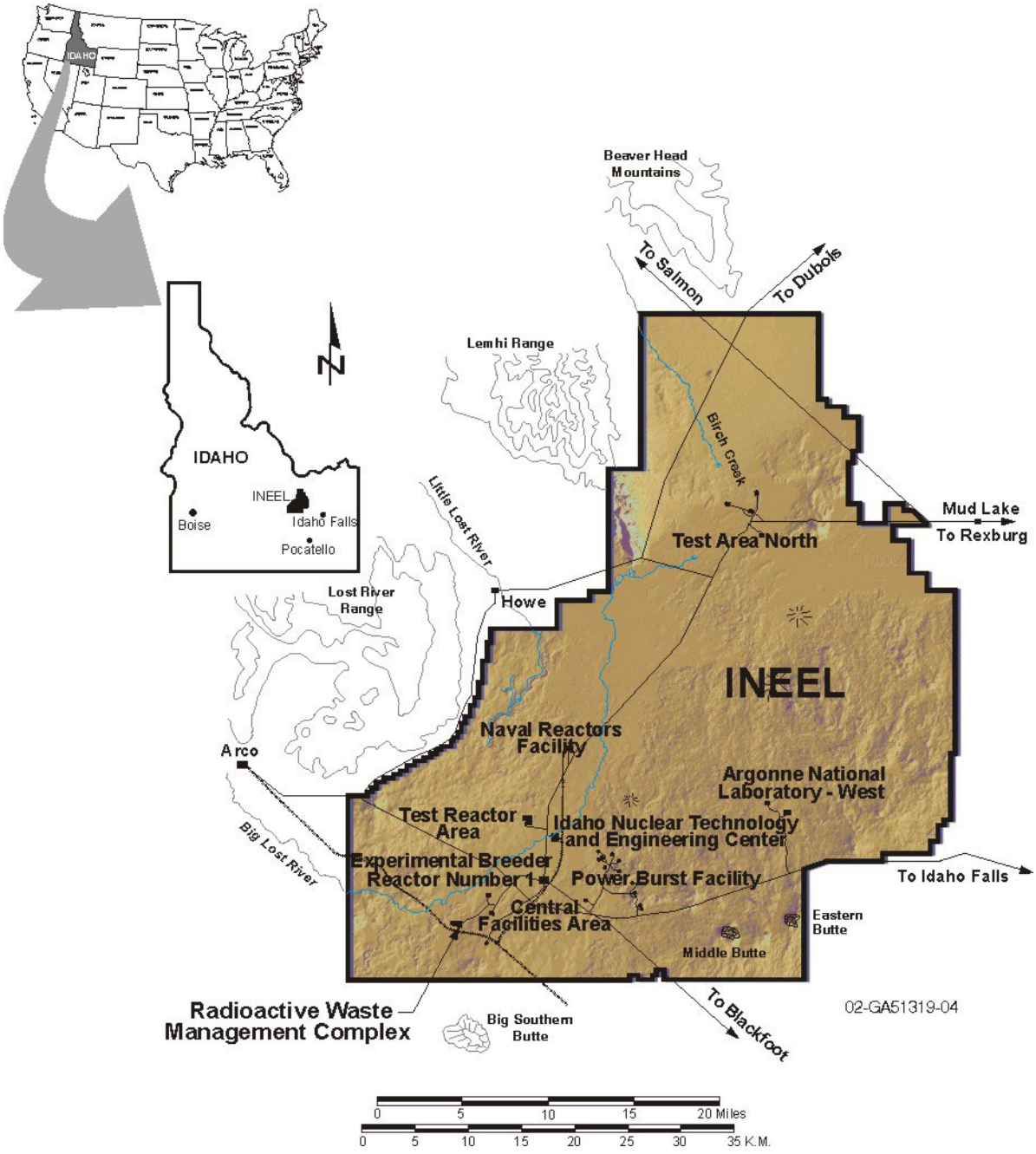

Figure 1. Location of the Radioactive Waste Management Complex and other major facilities at the Idaho National Engineering and Environmental Laboratory.

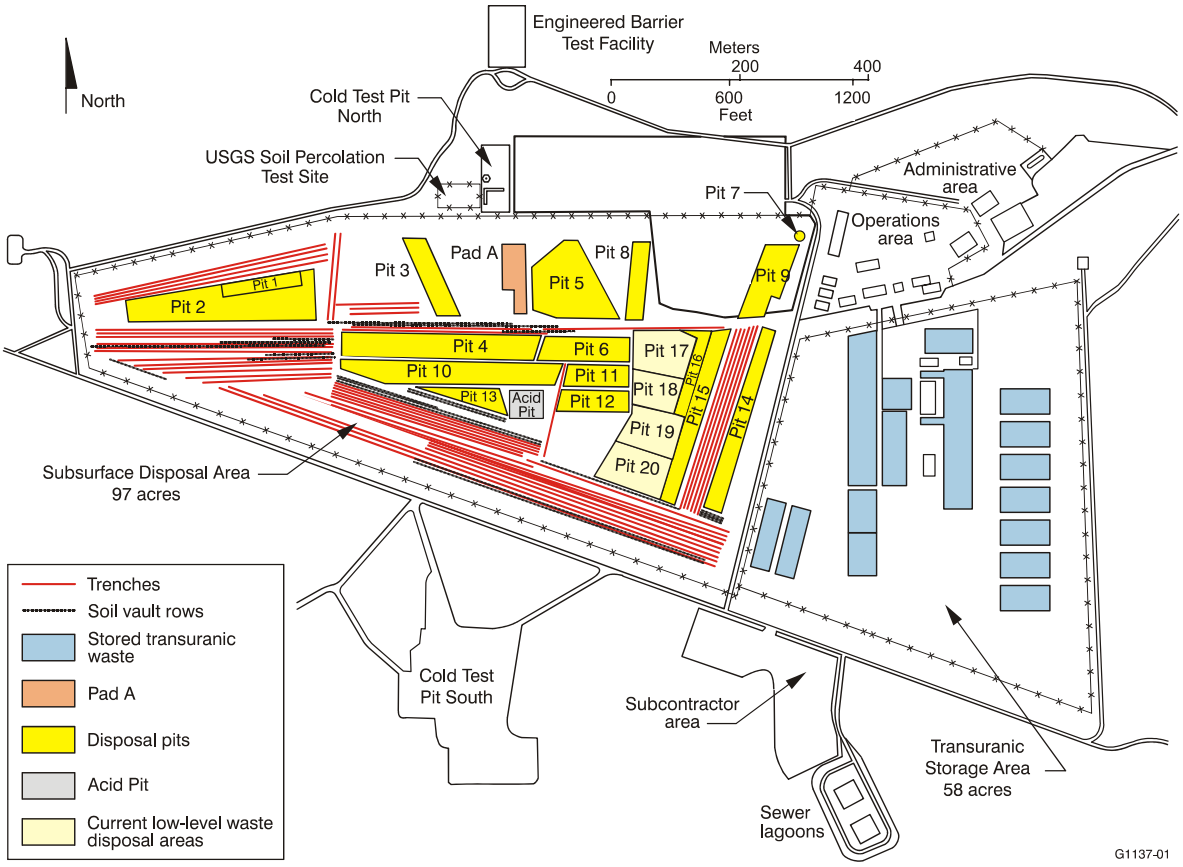

Figure 2. Map of the Radioactive Waste Management Complex showing the location of the Subsurface Disposal Area.

1.5 Document Organization

The following paragraphs briefly describe the remaining sections in this report.

Section 2 describes the relationship of this modeling effort to previous modeling and the basic approach to this work.

Section 3 describes the conceptual model.

Section 4 describes the 1-D numerical model.

Section 5 describes the 2-D numerical model.

Section 6 describes the limitations of the model.

Section 7 contains the summary and conclusions.

Section 8 provides the references used throughout this report.

Appendix A contains the 1-D input data file for SVR-20.

Appendix B contains the 2-D input data file for SVR-20.

2. RELATIONSHIP OF PROJECT TO PREVIOUS MODELING EFFORTS

A 1-D diffusion and advection model was developed by Art Rood (EDF-4835) to simulate the movement of HTO in the subsurface at SVR-20 (i.e., the beryllium disposal area). The HTO concentration measurements (Olson et al. 2003) were used to calibrate the HTO release rates in Rood's 1-D model. The concentrations were evaluated at three locations in the subsurface that corresponded to three closely related measurement ports. Since it was a 1-D model, the radial distances of the measurement ports from the source release nodes were not considered. The release rate of contaminants represented by this model only included ^{3}H that has moved laterally away from the soil vault auger hole. Three release points were modeled—2, 4, and 6 m—with the three release rates being calibrated to the measured concentration data. In the model, the average soil temperature was 9.7°C with an amplitude of 12.7°C. An average infiltration rate of 3.4 cm/year was used in the model. Rood suggested that future modeling work should employ:

- A 2-D model including unsaturated flow coupled with transport in the aqueous and vapor phase
- The model domain extending out some distance from the gas-sampling ports
- The model explicitly including the presence of canal baskets because they appear to control the horizontal migration of ^{3}H from the auger hole.

The recommendations (EDF-4835) for future model development have been incorporated into the present modeling study.

2.1 Overall Approach Used to Accomplish the Objectives

For this project, 1-D and 2-D models were developed using TETRAD—a multiphase, multicomponent simulator (Vinsome and Shook 1993; Shook 1995)—to simulate the contaminant release from the beryllium blocks into the subsurface porous media. Advection, molecular diffusion, adsorption, and radioactive decay mechanisms were incorporated into this model. Steady-state conditions initialization was performed before releasing contaminants in the simulations.

First, a 1-D model was developed and calibrated. Once the model was in good agreement with the estimated diffusion rates of HTO to the atmosphere based on monitored concentration in the air above the disposal location, sensitivity analysis of several model parameters was conducted to understand the effect of each parameter on contaminant transport. The 1-D model was extended radially to two dimensions. A 2-D, multiphase, multicomponent model was developed in cylindrical coordinates that allowed representation of the location of gas-sampling ports and explicit modeling of the basket as a barrier to horizontal migration of released contaminants. Locations of measurement cells in the model were representative of measurement ports installed around SVR-20. The 2-D model was calibrated to the HTO and $^{14}CO_2$ concentrations in the vadose zone obtained from several measurement ports. The soil properties (Van Genucten parameters) were obtained from Holdren et al. (2002), and basalt properties were obtained from Magnuson and Sondrup (1998). Predictive simulations were performed to estimate the amount of contaminants migrating into the soil and the atmosphere.

3. CONCEPTUAL MODEL

In this section, a description of the SVR-20 monitoring data, contaminants, and hydrogeologic and transport parameters is given.

3.1 Description of Soil Vault Row 20 and Monitoring Data

Figure 3 shows a photograph of the SVR-20 beryllium disposal location, which is the subject of this study. Figure 4 (adapted from Ritter and McElroy 1999) is a conceptual diagram of SVR-20. The auger hole is 1.5 m in diameter and 6.4 m in depth. A 0.6-m sediment layer is emplaced at the bottom of the auger hole. The auger hole contains three canal baskets, with each basket containing two irradiated beryllium blocks. The baskets were placed on top of each other with 0.15 m of soil layer in between. Bags made of Herculite were placed over the bottom of the cask during shipments. The canal baskets and the Herculite bags were discharged into the auger hole. The uppermost beryllium basket is 2 m below the surface. The baskets are constructed of galvanized sheet metal and measure 122 cm tall, 85 cm wide, and 74 cm deep (EDF-4835).

The engineering diagram for SVR-20, including the near-field subsurface region, is shown in Figure 5. A sediment layer exists to a depth of 6.2 m. Below the sediment layer is a highly fractured basalt region that offers low resistance to the flow of liquids. In summer, high air temperatures cause high rates of evapotranspiration, while in the winter, evapotranspiration rates are low. Infiltration estimates vary across the SDA from less than 1 cm/year to more than 30 cm/year (Holdren et al. 2002).

The monitoring data for the contaminants were obtained from the assessment in Olson et al. (2003). The contaminant concentrations were measured and reported over a 5-year period at various depths and distances from SVR-20 laterally in the soil and in the air at different heights above the disposal location (Olson et al. 2003). The monitoring equipment included suction lysimeters, thermistors, neutron access tubes, soil gas-sampling ports, and Type B probes (vapor sampling or tensiometers). In 1994, sampling wells and instrumentation were installed at SVR-20. Suction lysimeters, thermistors, and neutron access tubes were reasonably assumed to be placed 30 cm outside the auger hole at 2 m and 6 m below grade. Ports for soil gas sampling were placed approximately 30 cm outside the auger hole at 2.7, 4.5, and 6.2 m below grade in gas-sampling port Well-1. The Type B probes (configured as either vapor sampling or tensiometers) were placed at greater distances from the buried beryllium in SVR-20 to monitor the lateral migration of HTO and $^{14}CO_2$. A Type B vapor port is located 5 m away from SVR-20 at a depth of 5.4 m. Contaminants that moved downward below SVR-20 were not measured.

3.2 Contaminant Description

The primary contaminant of concern is ^{14}C, and the contaminant of interest present in activated beryllium is ^{3}H. The six beryllium blocks contain an estimated 114,800 Ci of tritiated hydrogen gas and 11.95 Ci of ^{14}C (Mullen et al. 2003). The specific activity of carrier-free ^{3}H is 9.696E+3 Ci/g and of carrier-free ^{14}C is 4.46 Ci/g. The ^{3}H concentration in beryllium was estimated to be about 3 Ci/cm^3, decreasing by a factor of 2 for every 2.5 cm away from the surface of the beryllium that was closest to the ATR fuel. The specific activities were used to convert the block inventory into contaminant mass, to convert back the model-predicted contaminant concentrations in molar fraction units, and to convert diffusion in mass rates to activity units.

Figure 3. View of the location at Soil Vault Row 20 where activated beryllium blocks were buried in 1993.

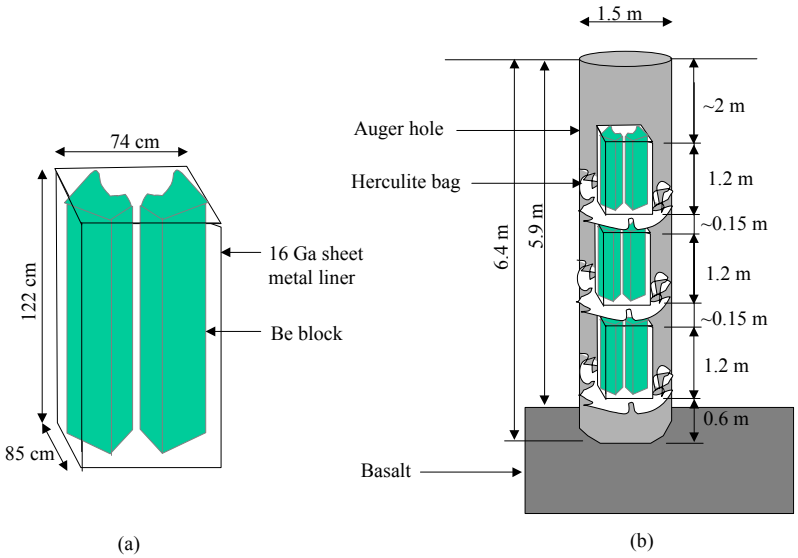

Figure 4. Conceptual diagram of Soil Vault Row 20.

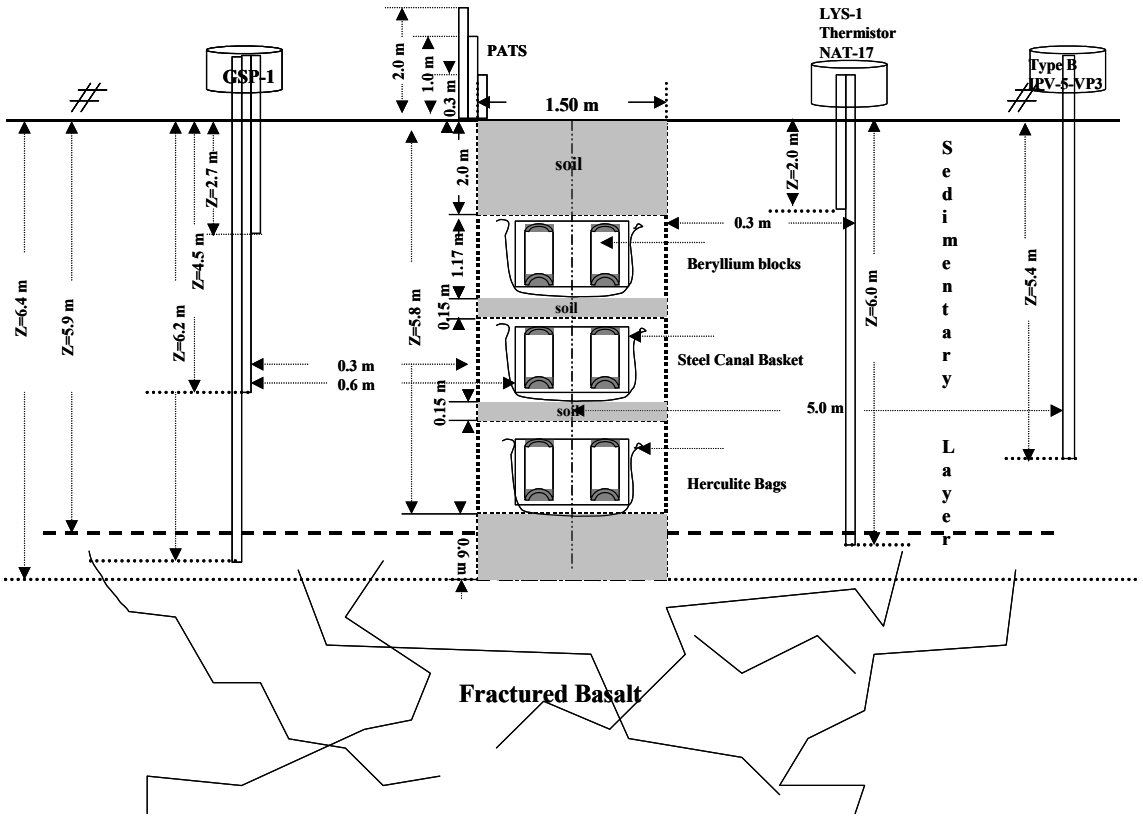

Figure 5. Engineering diagram for the model for Soil Vault Row 20.

Before disposal, the beryllium blocks were used as reflectors in the ATR. During the intense neutron irradiations, ^{3}H and ^{14}C were produced in the beryllium blocks. Beryllium in contact with soil corrodes, leading to a release of ^{3}H and ^{14}C. The beryllium corrosion rate was reported to be 1 mm in 39.37 years or 2.65E–3/year (Adler Flitton et al. 2001). Tritium is released from the corroding beryllium block as elemental ^{3}H (i.e., ^{3}H or T_2) and quickly oxidizes to HTO (i.e., $^{3}HO^{1}H$ vapor), while ^{14}C released from the beryllium blocks oxidizes to $^{14}CO_2$. Molecular diffusion, advection caused by infiltration, and adsorption onto the soil surface are the major processes that affect migration of contaminants. The HTO does not react with the soil solid phase, while $^{14}CO_2$ reacts with the soil solid phase. Tritiated water partitions into both the gaseous and aqueous phases. Radioactive $^{14}CO_2$ is highly mobile, partitions into both the vapor and liquid phases, and undergoes adsorption onto soil.

3.3 Hydrogeologic and Transport Parameters

The porosity and hydraulic conductivity values were obtained from inverse modeling and estimation of hydraulic properties at the SDA, including the SVR-20 location. Based on the inverse parameters obtained at two locations in the vadose region, the model subdivides the soil portion into two different sedimentary layers. The top sediment extends from the surface to a depth of 4.76 m. The bottom sedimentary layer extends from 4.76 to 5.55 m. The basalt formation starts at a depth of 5.55 m. The surface elevation is 1,527 m. The fractured basalt section was modeled as a single-porosity medium with linear relative permeability. It had low residual liquid water saturation, simulating easy drainage of fluids. For the sedimentary layer, Van Genuchten curves characterizing relative permeability and capillary pressure of the sedimentary layers are given in Table 1 (Holdren et al. 2002). The parameters for the fractured basalt layer relative permeability curve are given in Table 2.

Table 1. Sedimentary hydraulic and relative permeability parameters.

Inverse of air entry value, α (1/cm)	1.066
Pore size distribution index, n (–)	1.523
Residual water saturation, S_{wr}	0.292
Residual gas saturation, S_{gr}	0.0
Residual oil saturation, S_{or}	0.05
Permeability in horizontal direction, mD	680.0
Permeability in vertical direction, mD	680.0
Porosity	0.5
Interfacial tension, σ_{ow} (N/m)	1.0
Interfacial tension, σ_{go} (N/m)	0.0
Interfacial tension, σ_{gw} (N/m)	1.0

(Holdren et al. 2002)

Table 2. Basalt hydraulic and relative permeability parameters.

Residual water saturation, S_{wr}	0.0001
Residual gas saturation, S_{gr}	0.01
Residual oil saturation, S_{or}	0.0
Permeability in horizontal direction, mD	9,000.0
Permeability in vertical direction, mD	300.0
Porosity	0.05
End point relative permeability for water	1.0
End point relative permeability for gas	1.0
Exponent for water relative permeability	2.0
Exponent for gas relative permeability	1.2
End point oil water capillary pressure, kPa	32.0
End point gas oil capillary pressure, kPa	0.0
Exponent for oil water capillary pressure	1.5
Exponent for gas oil capillary pressure	1.0

(Magnuson and Sondrup 1998)

3.3.1 Transport Parameter Estimation

The mathematical formulation for estimating the various transport parameters is described in this section. The mechanisms involved in the transport of contaminants include advection and diffusion in the gaseous and aqueous phases, dispersion caused by mixing, adsorption onto the solid phase, and sources or sinks. In this specific case, the transport phenomena governing the migration of HTO and $^{14}CO_2$ are diffusion in the aqueous and gaseous phases, advection with the infiltrating water, and adsorption onto the solid surface (i.e., adsorption for $^{14}CO_2$ alone). The basis for obtaining the transport parameters will be discussed in Sections 3.3.1.1 and 3.3.1.2. The transport parameters used for modeling SVR-20 are shown in Table 3.

Table 3. Transport parameters used in the Soil Vault Row 20 model.

Parameter	Species	Value	Reference
Molecular diffusion coefficient in gaseous phase, D_g	Tritiated water	2.22 m^2/day	(Smiles, Gardner, and Schulz 1993; Rose 1966)
Molecular diffusion coefficient in gaseous phase, D_g	$^{14}CO_2$	1.6 m^2/day	(Hull and Hohorst 2001)
Tortuosity		Millington-Quirk formulation (function of air-filled porosity and total porosity)	
Molecular diffusion coefficient in aqueous phase, D_w	Tritiated water	19.53E–5 m^2/day	(Smiles, Gardner, and Schulz 1993; Sposito 1981)
Molecular diffusion coefficient in aqueous phase, D_w	$^{14}CO_2$	4.32E–5 m^2/day	(Flickinger and Drew 1999)
Equilibrium ratio (mole fraction in vapor phase to liquid phase)	Tritiated water	1.347E–2 at 84.8 kPa and 10°C	(TETRAD User Manual [Version 13])
Equilibrium ratio (mole fraction in vapor phase to liquid phase)	$^{14}CO_2$	3.4198E+2 at 84.8 kPa and 10°C	(EDF-3394)
Adsorption coefficient, K_d	$^{14}CO_2$	0.8 mL/g	(Hull and Hohorst 2001)

3.3.1.1 Diffusion. Transport mechanism by diffusion in the gaseous phase is described by Fick's Law, which states that the diffusion rate is proportional to the concentration gradient in the gaseous phase, and the constant of proportionality is the effective diffusion coefficient. The effective diffusion coefficient is a function of the free-air diffusion coefficient (D_o), gas-filled porosity (θ_g), total porosity (θ), and the property of the medium called the tortuosity (τ_g). The effective diffusion coefficient is given by an expression derived by Millington (1959) and is shown in Equation (1):

$$D_{eff} = \frac{D_o \theta_g}{\tau_g} \tag{1}$$

where

$$\tau_g = \frac{\theta^2}{\theta_g^{7/3}} \quad .$$

The tortuosity calculated for the 2-D basecase model (the results are described in Section 4.3) is shown below. The total porosity in the top sediment (i.e., 4.76 m) was 0.61, and the average aqueous-phase saturation in the top sediment was 0.59. The water-filled porosity was calculated to be 0.36, and the air-filled porosity was calculated to be 0.25. The average tortuosity (τ_g) in the top sediment was calculated to be 9.45. The average effective gaseous-phase diffusion coefficient was calculated to be 0.0587 m^2/day for HTO and 0.0423 m^2/day for $^{14}CO_2$. The diffusion coefficient for the aqueous phase is approximately four to five orders of magnitude lower than diffusion coefficients for the gaseous phase.

3.3.1.2 Partitioning between the Phases. The equilibrium ratio is defined as the ratio of the moles of species *i* in the vapor phase to the moles of species *i* in liquid phase. For species at low concentration in aqueous phase, Henry's Law holds good and is used to calculate the equilibrium ratios. The Henry's Law constant is the ratio of vapor pressure to solubility; therefore, it is a measure of the partition of the species between the vapor phase and aqueous phase. At equilibrium, the fugacity of the species in the liquid phase is equal to the fugacity of the species in the aqueous phase. When a gas is only sparingly soluble in a liquid (i.e., as $x_1 \rightarrow 0$), the liquid-phase mole fraction of the solute species is linearly proportional to its gas-phase fugacity (shown in Equations [2] and [3]) (Sandler 1989).

$$x_1 H_1(T,P) = y_1 P\left(\frac{f}{p}\right)_1 \tag{2}$$

At low pressures, $\left(\frac{f}{p}\right)_1$ approaches 1;

therefore, $H_1(T,P) = \left(\frac{y_1}{x_1}\right)P$ (3)

where

$H_1(T,P)$ is the Henry's Law constant at that temperature and pressure.

The mole fraction in the gaseous phase to the aqueous phase is defined in TETRAD as the AKVAL. The Henry's Law constant can be determined from the AKVAL using Equation (3). The AKVAL in TETRAD is calculated as a function of temperature and pressure as follows in Equation (4):

$$\begin{aligned} Y_i &= AKVAL * W_i \\ AKVAL &= (A / P_{ABS} + B + C * P_{ABS}) * \exp\left(-D \middle/ (T_{ABS} - E)\right) \end{aligned} \quad . \tag{4}$$

The HTO component is treated as having the same equilibrium ratio of partitioning between aqueous and gaseous phase as in a pure water component. The value of AKVAL for HTO was 1.347E–2 at 84.8 kPa and 10°C. The corresponding Henry's Law constant was 1.142 kPa. For $^{14}CO_2$, the value of the TETRAD A parameter was initialized to $2.9*10^4$ kPa (EDF-3394); the rest of the parameters (i.e., B, C, D, and E) were initialized to zero. The value of AKVAL for $^{14}CO_2$ was 3.4198E+2 at 84.8 kPa and 10°C. The respective Henry's Law coefficient was calculated to be $2.9*10^4$ kPa.

Partitioning of a component between the aqueous phase and the solid phase is defined by the adsorption relationship. In this model, a linear adsorption relationship was used to define the fraction mass of component adsorbed from the aqueous phase per mass of soil as given in Equation (5):

$$F_{ads} = A(S_w W_{iw}) \tag{5}$$

where

F_{ads} = the fraction mass of component adsorbed from a phase per mass of soil

S_w = aqueous-phase saturation

W_{iw} = mole fraction of component i in the aqueous phase.

The model incorporated the adsorption of $^{14}CO_2$ into the soil phase, and the adsorption coefficient for $^{14}CO_2$ is 0.8 mL/g (Hull and Hohorst 2001).

4. TETRAD AND ONE-DIMENSIONAL NUMERICAL MODEL DESIGN

TETRAD is a three-dimensional, three-phase simulator capable of solving the transport of contaminants in subsurface media, both porous and fractured. TETRAD allows modeling the effects of gravity, capillarity, advection, dispersion, adsorption onto the soil surface, equilibrium partitioning between liquid and vapor, and radioactive decay. The governing equations are the mass conservation equation for each component *i*. The components of interest in this model are pure water, HTO, and radioactive carbon dioxide. In the model, the contaminants are treated as tracers because they are present in significantly small concentrations and do not affect the physical properties of the fluids. The boundary conditions that can be defined in TETRAD are the Dirichlet boundary condition (i.e., constant pressure, as in atmospheric pressure boundary), Neumann boundary condition (i.e., specified flow rate such as in surface water infiltration flux or aquifer influx), and mixed boundary condition (i.e., constant pressure and rate combined). More details on the formulation and validation of TETRAD for environmental applications can be found in Shook (1995). The following sections describe the development, calibration, and sensitivity analysis of the 1-D numerical model.

4.1 Space and Time Discretization

The 1-D numerical model developed for SVR-20 is presented in Figure 6 and the gridding scheme used for the 1-D model is shown in Figure 7. The domain size was $1 \times 1 \times 48$, with 48 representing the grids in the z direction (i.e., vertical). The top 12 cells are assigned parameters representative of the top sedimentary layer, cells 13 to 35 are assigned parameters representative of the beryllium-enclosed basket, and cells 36 to 39 are assigned parameters representative of the bottom sedimentary layer followed by the fractured basalt section to the domain bottom. Space was discretized vertically in the sedimentary layer with a uniform grid size of 0.166 m and was increased subsequently by a factor of 1.5 in. the fractured basalt region. The domain size in the z direction was 18.91 m, while in the x and y directions, it was 1.33 m in either direction. The cross section of the auger hole with a radius of 0.75 m was equivalent to the Cartesian 1-D model with dimensions of 1.33 m of each grid block side. The cells representing beryllium-enclosed baskets were assigned a porosity of 0.95 and a permeability of 100 mD. The 1-D model did not take into account the presence of 0.15-m-thick soil layer between the baskets. Time stepping was done automatically based on the residuals and the set norms. The initialization period was 100,000 days, and after a steady state was attained, the cells representing beryllium enclosed baskets started to release the contaminants into the soil. A fully implicit scheme was adopted to solve the system of equations. The Van Genuchten curve parameters characterizing the relative permeability and capillary pressure of soil in the vadose zone are shown (mentioned in previous sections) in Table 1. A summary of the parameters used for the 1-D model is given in Table 4.

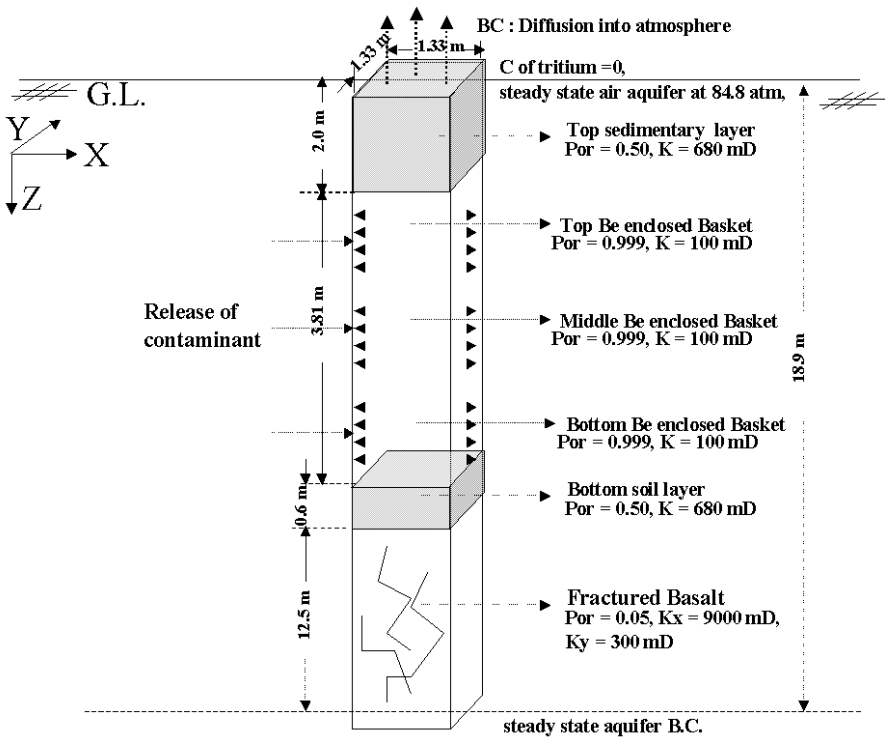

Figure 6. One-dimensional model representing the release and transport of contaminant from buried beryllium blocks in Soil Vault Row 20.

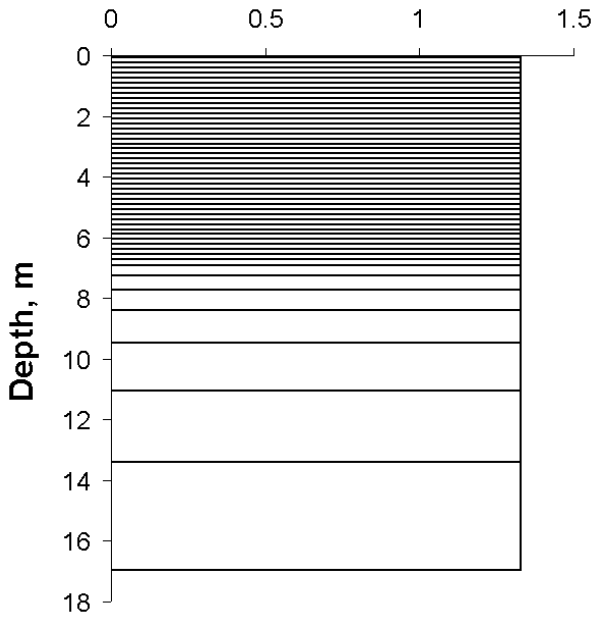

Figure 7. Spatial grid discretization used for the one-dimensional model.

Table 4. Summary of parameters for one-dimensional model.

Grid Dimensions, NX × NY × NZ	1 × 1 × 48
Dx (m)	0.166
Dy (m)	0.166
Dz (m)	39 39*0.166 1 0.166 1 0.249 1 0.3735 1 0.5602 1 0.8404 1 1.2605 1 1.8908 1 2.8363 1 4.2544
Porosity	Gridblocks 1 to 12 (0.61) Gridblocks 13 to 35 (0.95) Gridblocks 36 to 39 (0.39) Gridblocks 40 to 48 (0.05)
Permeability (mD)	104.675 (1 to 12) 100 (13 to 35) 21.564 (36 to 39) 300 (40 to 48)
Boundary Conditions Top Surface Bottom Surface	 Air pressure of 84.8 kPa Air pressure of 85.2 kPa
Steady Infiltration Rate (cm/year)	1.0

4.2 Model Boundaries

The model focuses on the surface sedimentary layer of 6.4-m thickness. The bottom boundary condition was assigned at a depth of 18.94 m below the surface. The top boundary was assigned a mixed-boundary condition with an atmospheric pressure of 84.8 kPa (i.e., steady-state air aquifer) and a constant water infiltration rate of 1 cm/year. The vapor-phase static pressure gradient was assumed to be 0.0104 kPa/m, which is consistent with pressures at an elevation of 1,524 m.

The bottom boundary condition is constant pressure (Dirichlet boundary condition). The boundary condition was far enough away to not influence the transport of contaminants near the source. Constant aqueous-phase pressure corresponding to initial 90% saturation is maintained. Therefore, a constant

pressure boundary condition at the bottom ensured that when aqueous-phase saturation increased in the bottom layer because of downward fluid advection, capillary pressure decreased, and aqueous-phase pressure increased. The fluid outflow rate at the bottom, defined by Darcy's Law, would be directly proportional to the aqueous-phase pressure difference between the bottom layer and the boundary-specified constant pressure. This fluid outflow modeled downward infiltration of liquid water. Aqueous-phase contaminants would be able to migrate out at the domain bottom, predominantly through aqueous-phase advection.

Contaminants were allowed to diffuse at the soil-air boundary, but the diffusion boundary condition was not specified at the domain bottom. Advection in this model is downward because of infiltration, and therefore, aqueous-phase contaminant downward migration is primarily influenced by advection. Advection does not occur in the upward direction, and diffusion becomes an important mechanism to describe upward transport of contaminants. The driving force in diffusion is the concentration gradient. The concentration gradient would be substantial near the source release and, hence, would be more predominant in surface sediments near the source. At greater distances from the source release, concentration gradients become smaller, and diffusion becomes negligible. The diffusion rate through the near-saturated bottom layer would be very small because near saturation is forced in that layer. In the field, fine-grained, moist interbed sedimentary layers would be a very effective barrier to gas diffusion. The bottom boundary condition is representative of sedimentary layers, and therefore, a diffusion boundary condition was not included at the domain bottom.

4.3 One-Dimensional Model Calibration

The calibration target for the 1-D model is the diffusion rate of HTO into the atmosphere. This total diffusion rate (or emission) is estimated from HTO strengths measured at various heights above the auger hole and using a box model with reasonable estimates of annual average windspeed and box dimensions (Olson et al. 2003). Diffusion is the predominant transport mechanism for HTO migration upward into the atmosphere from the top layer of soil gas. In the early simulation stages, the soil aqueous-phase saturation was variable (transient state) based on the variable surface water infiltration rates and advective drainage, but steady-state conditions were established by running the simulation for 100,000 days before releasing the contaminants in the model. Time zero in the model corresponds to the date July 31, 1993. After the release of contaminants, the infiltration rate was kept constant at 1 cm/year, which was judged to be a reasonable rate. The estimated source release rate data of ^{3}H and ^{14}C (expressed in Curies/day) were obtained from Holdren et al. (2002) and are plotted in Figure 8. In the plots, "H-3" refers to HTO, and "C-14" refers to $^{14}CO_2$. The 1-D model HTO diffusion rate (expressed in Curies/day) into the atmosphere was compared with the estimated diffusion rate in Figure 9, and a reasonable agreement was obtained. The model-predicted diffusion rates were one to two orders of magnitude below the estimated HTO diffusion rates into the atmosphere. The measured HTO diffusion rate into atmosphere included both the summer and winter monitoring data, while the model assumed an isothermal temperature of 10°C. The model does not account for the seasonal behavior of flux to the atmosphere. Figure 10 compares the 1-D model profile of moisture content with the NAT-17 measured data for April 1997. The NAT-17 measuring port was located 0.3 m radially away from the outer surface of the auger hole. However, the 1-D model does not take into account the radial distance between the auger hole and the NAT-17 measuring port as it simulates only the flow and transport in the z direction and also does not account for the presence of 0.15-m-thick soil layers between baskets. Therefore, the cells representing the beryllium blocks do not agree well in the moisture content profile with the measured data, but the cells representing the top sedimentary layer have reasonable agreement with the measured data.

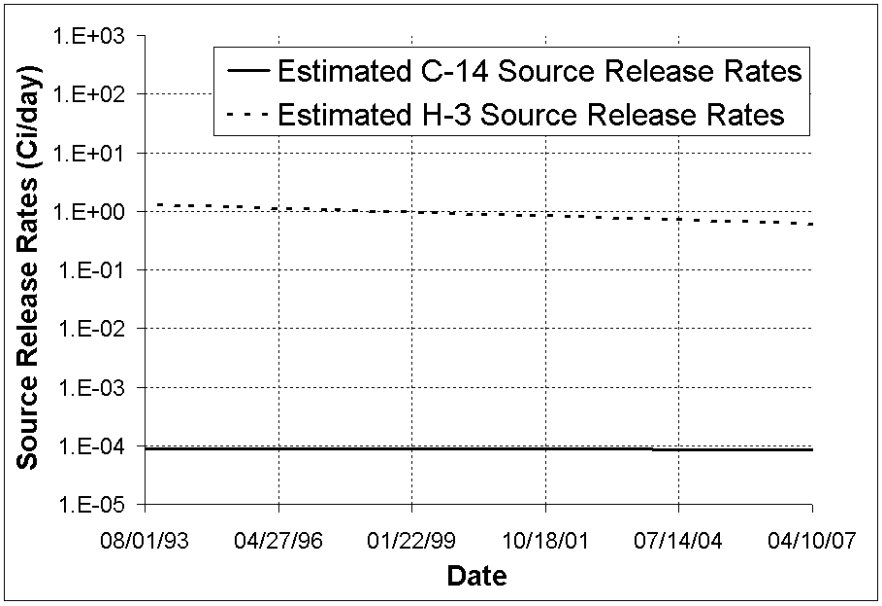

Figure 8. Estimated source release rates of carbon-14 and tritium from the irradiated beryllium blocks.

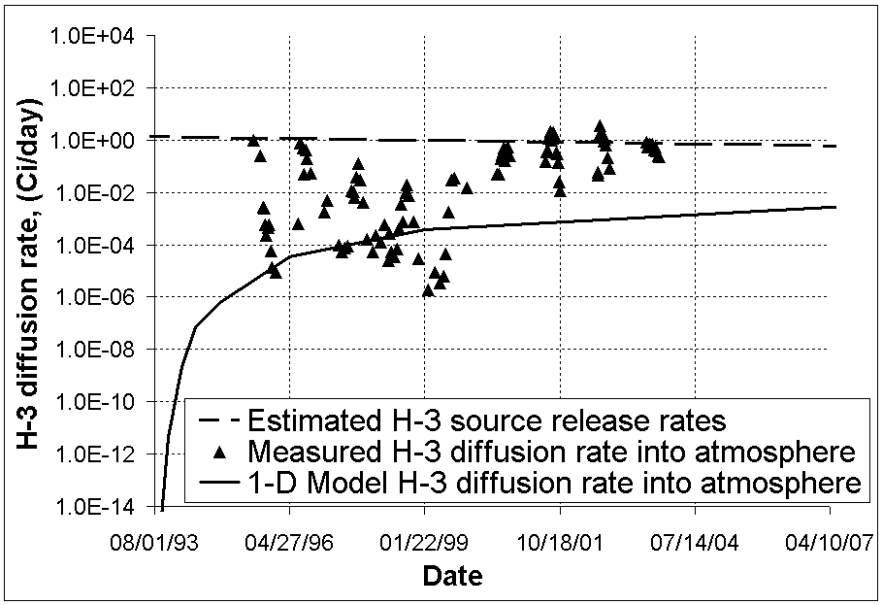

Figure 9. Comparison of one-dimensional model predicted with estimated tritiated water diffusion rates (based on measurements) into atmosphere; also plotted is the tritiated water source release rate.

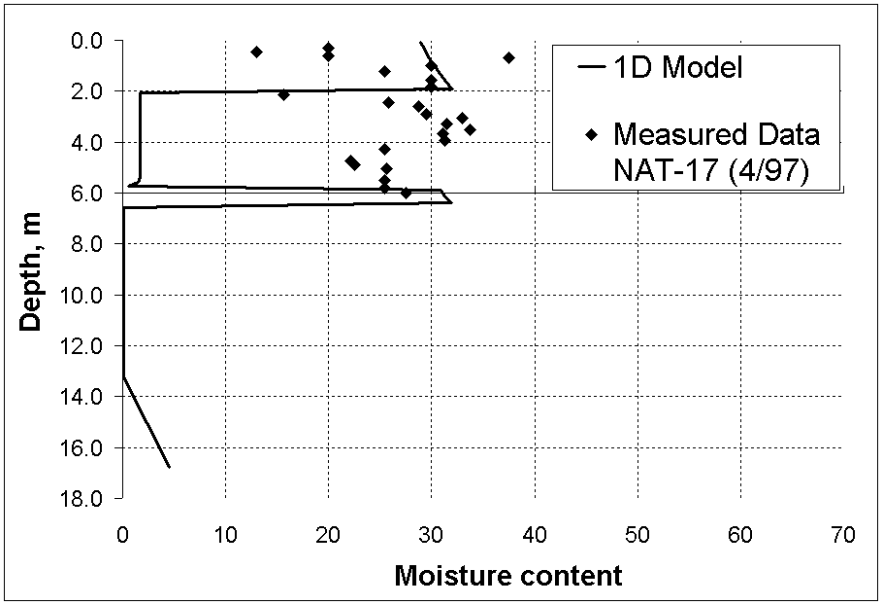

Figure 10. Comparison of one-dimensional model moisture content profile with NAT-17 measured data on April 1997.

The molecular diffusivities of HTO in gaseous and aqueous phases were obtained from literature (Smiles, Gardner, and Schulz 1993). Tortuosity in each grid block was calculated based on the Millington-Quirk formulation. Based on the total porosity of 0.61 and a liquid water saturation of 0.59 (in the top sediment), the average tortuosity (τ_g) was calculated to be 9.45. As the infiltration rate was lowered, the diffusion rate of HTO to atmosphere increased. An infiltration rate of 1 mm/year gave a much better agreement of the model with the estimated diffusion rates, while an infiltration rate greater than 1 cm/year lead to greater differences in the model and estimated diffusion rates. Since 1 cm/year was considered to be a reasonable infiltration rate, the calibrated model adopted this rate at the expense of a better agreement with the monitored data for a lower than 1-cm/year infiltration rate. The model was calibrated through the infiltration rate. The sensitivity study conducted on the 1-D model is discussed in the following sections.

4.4 One-Dimensional Model Prediction

In Figure 11, the model-predicted $^{14}CO_2$ diffusion rate into the atmosphere is compared with the estimated $^{14}CO_2$ source release rate. In the 1-D model, the contaminants do not migrate laterally. These contaminants migrate only in the z direction, leading to an overestimation of the diffusion rate into the atmosphere. The diffusion rate of $^{14}CO_2$ into atmosphere increases nonlinearly initially (approximately 3 years) and reaches a pseudo steady state for the next 10-year simulation period (i.e., variation in the diffusion rate of $^{14}CO_2$ to the atmosphere is small over time).

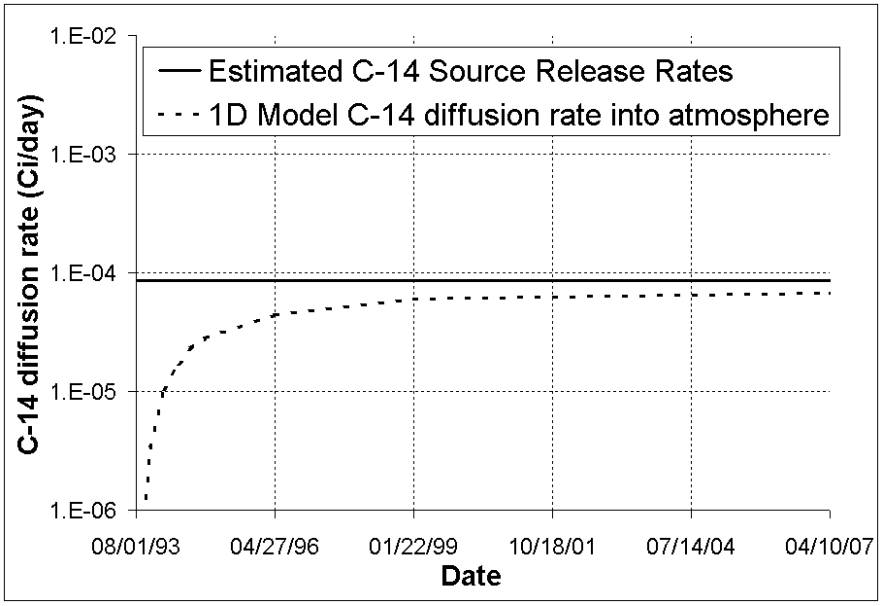

Figure 11. Comparison of one-dimensional-model-predicted $^{14}CO_2$ diffusion rate into atmosphere with source release rate.

4.5 One-Dimensional Model Sensitivity Analysis

Several different parameters were varied, and an understanding of the variation of parameter on the HTO diffusion rates into the atmosphere was studied. Sensitivity studies of barometric pumping effects, infiltration rates, relative permeability effects, and residual water saturation were conducted and are presented below. These studies also contributed to the development of a calibrated 1-D model.

4.5.1 Barometric Pumping Effects

The basecase was modified to include barometric pumping with a cyclic amplitude of 1.4 kPa for a period of 10 days throughout the simulation period. Figure 12 plots the HTO diffusion rate into the atmosphere with and without the barometric pumping. The barometric pumping did not have a significant effect on HTO diffusion rates. The barometric pumping effects are described in relevance to 18.9-m-thick porous media only.

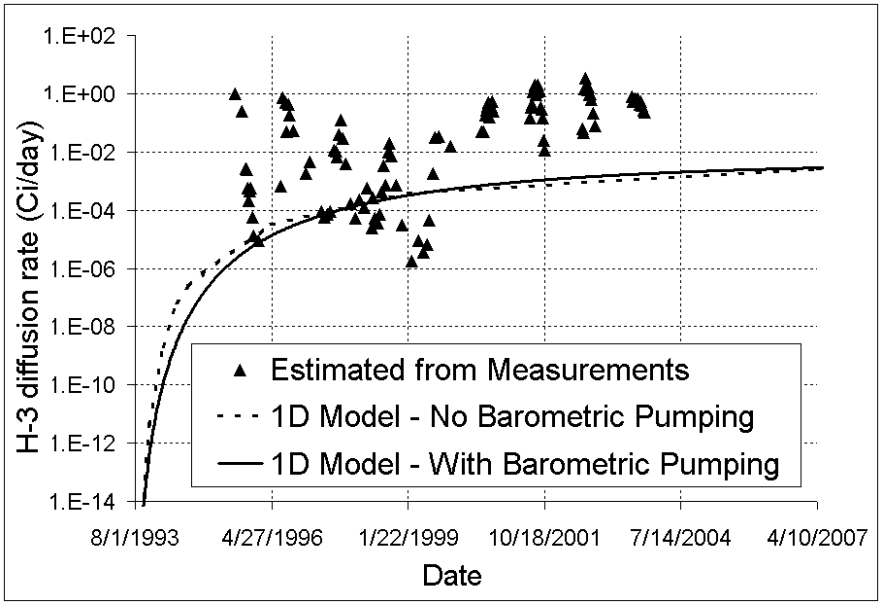

Figure 12. One-dimensional model-predicted tritiated water diffusion rate into the atmosphere with and without barometric pumping.

4.5.2 Infiltration Rate

The effects of varying the infiltration rates on HTO diffusional migration into the atmosphere were studied. The basecase had a steady infiltration rate of 1 cm/year. In the sensitivity study, three cases were compared with the basecase. Case A had an infiltration rate of 10 cm/year for 10 days/year with zero infiltration in the remainder of the year (i.e., 0.274 cm/year annual average), and Case B had 36.5 cm/year for 10 days/year with zero infiltration in the remainder of the year (i.e., 1 cm/year annual average). The effects of different infiltration rates on the diffusion rate of HTO and C-14 into the atmosphere are shown in Figure 13 and Figure 14, respectively. The plot shows that, with lower infiltration rates, HTO diffusion rate into atmosphere increases significantly. Thus, the infiltration rates have a significant effect on HTO diffusion rates into the atmosphere. As the infiltration rate increases, aqueous-phase saturation in the soil above the beryllium blocks increases, resulting in an advective dominant flow. Decrease in the air-phase saturation would result in a decrease of the diffusion rate of HTO into the atmosphere.

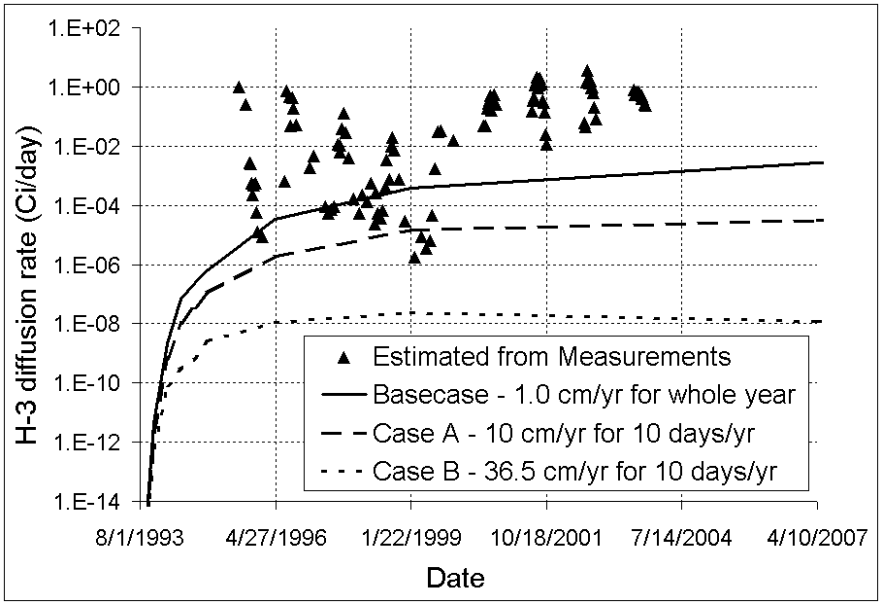

Figure 13. Comparison of tritiated water diffusion rates into the atmosphere for different infiltration rates.

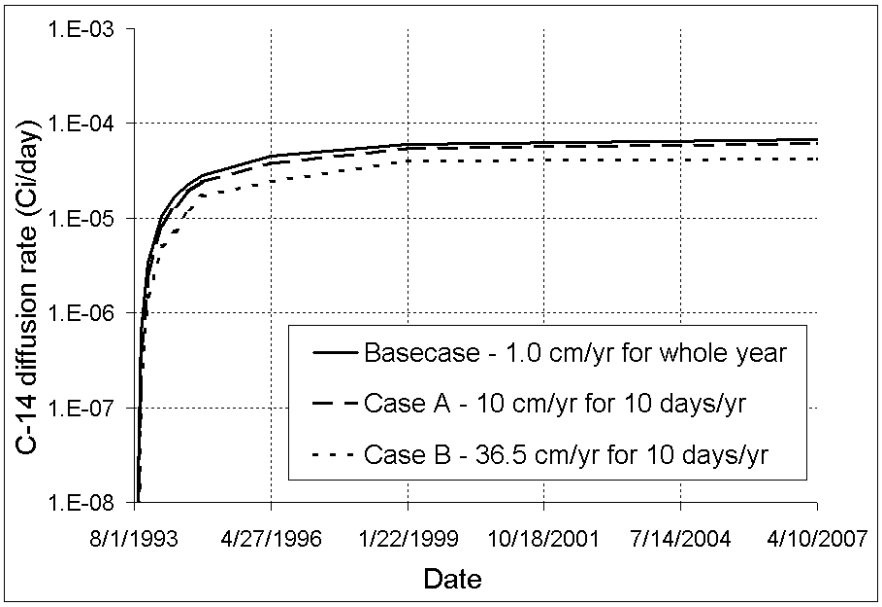

Figure 14. Comparison of $^{14}CO_2$ diffusion rates into atmosphere for different infiltration rates.

4.5.3 Residual Water Saturation Effects

The residual liquid water saturation was changed from 0.275 to 0.05, and its effects on the HTO diffusion rate were studied. The basecase relative permeability given in Table 1 was used. The results are shown in Figure 15. As the residual water saturation decreased, the average soil moisture in the top sediment also decreased. The resulting increase in the vapor-phase saturation allowed an increase in the diffusion rate of HTO into the atmosphere by an approximate factor of 3.

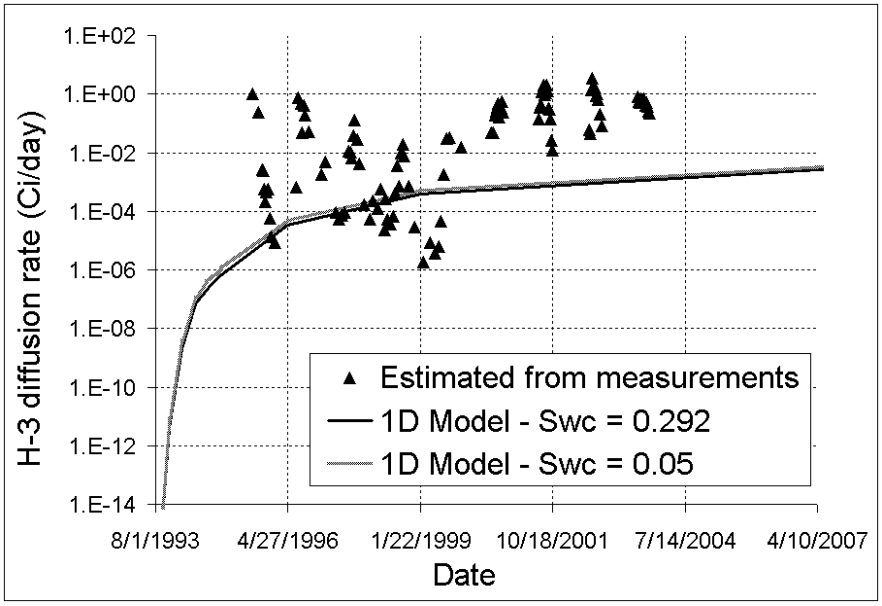

Figure 15. The tritiated water diffusion rates for two different residual water saturations.

5. TWO-DIMENSIONAL NUMERICAL MODEL DESIGN

Using the calibrated 1-D model as a basis, the SVR-20 model was extended from a 1-D to 2-D radial model. In the 2-D model, the contaminants released from the enclosed baskets could potentially migrate upward into the atmosphere, laterally into the vadose zone soil layer, and downward into the fractured basalt. The contaminant concentration measuring ports are located both laterally away from the beryllium blocks in the soil and above ground surface of the disposal location. These lateral contaminant monitoring ports provide further sets of data to calibrate the 2-D model, which was not used for the calibration of the 1-D model. The schematic diagram of the SVR-20 conceptual 2-D cylindrical coordinate model is given in Figure 16. The gas-sampling ports (i.e., GSP-1) are shown as M1, M2, and M3 in the conceptual diagram. These ports also are referred to as 2M, 4M, and 6M, indicating their depths, respectively. The model had a sedimentary layer in the top with fractured basalt below. The model extends radially to 6 m and vertically to 18.9 m. The monitoring port IPV-5 is located 5 m away from the axis of the auger hole.

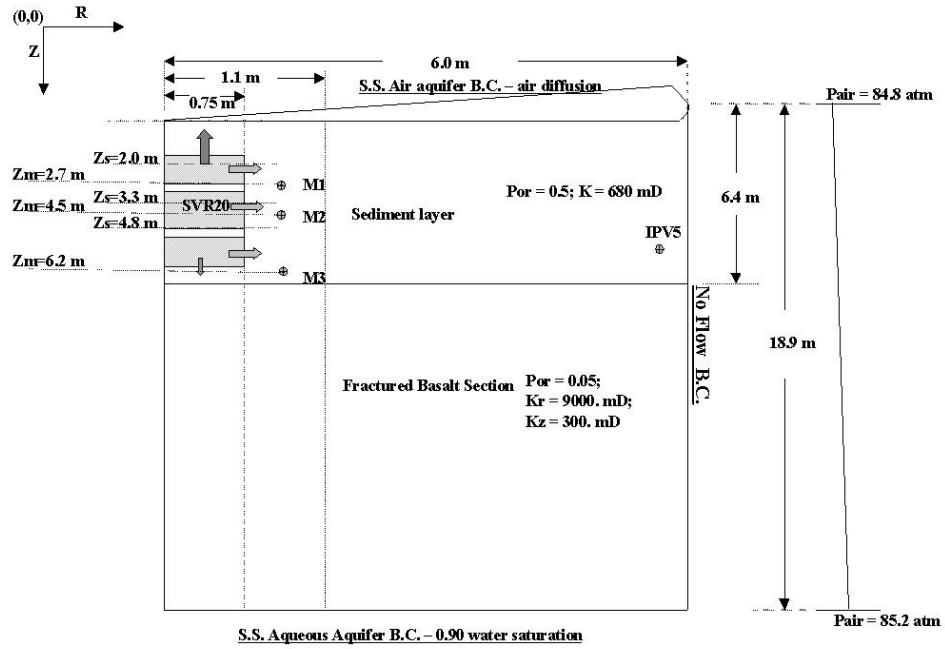

Figure 16. Two-dimensional model of Soil Vault Row 20.

5.1 Space and Time Discretization

The domain of the 2-D model has 11 radial grid blocks and 48 grid blocks in the vertical direction. The first three radial grid blocks, with a total radius of 0.75 m, correspond to the auger hole. The next 0.05-m-thick radial grid represents either the basket wall, which is a barrier to lateral diffusion where present, or soil. The rest of the radial grids represent the soil layer in the top portion of the model domain and fractured basalt in the bottom portion of the model domain. Figure 17 shows the spatial grid discretization used in the 2-D model. A constant vertical grid size of 0.166 m is used for the top 6.4 m representing the soil layer, and below that, the vertical grid size is increased by a factor of 1.5 representing the fractured basalt. An automatic time-stepping routine is used based on the norms and

residuals. The numerical model is discretized into 48 layers. The top 39 grid layers represent the soil layer, while the bottom nine grid layers represent the fractured basalt. The soil vault row is subdivided vertically into three subsections representing the three baskets containing the beryllium blocks. The top basket extends from the 13th to the 19th layers, the middle basket extends from the 21st to the 27th layers, and the bottom beryllium blocks basket extends from 29th to 35th layers with the intermittent layers representing 0.15-m-thick soil sediment. The cells representing the barriers to lateral diffusion along the edges of the three baskets are assigned a porosity and permeability of 0.0, thereby preventing the molecular diffusion radially through these cells. The top and bottom of the baskets are open to diffusion of the released contaminant; therefore, the intermittent soil layers form the pathways for the transport of contaminants laterally into the vadose zone. The cells representing the beryllium blocks are assigned a porosity of 0.95, air saturation of 0.99, and an isotropic permeability of 100 mD. The cells representing the soil and fractured basalt are initialized to an air saturation of 0.1 and aqueous-phase saturation of 0.9 with a porosity of 0.5 in the sediment and 0.05 in the fractured basalt. A constant infiltration rate of 1 cm/year was assigned to the model.

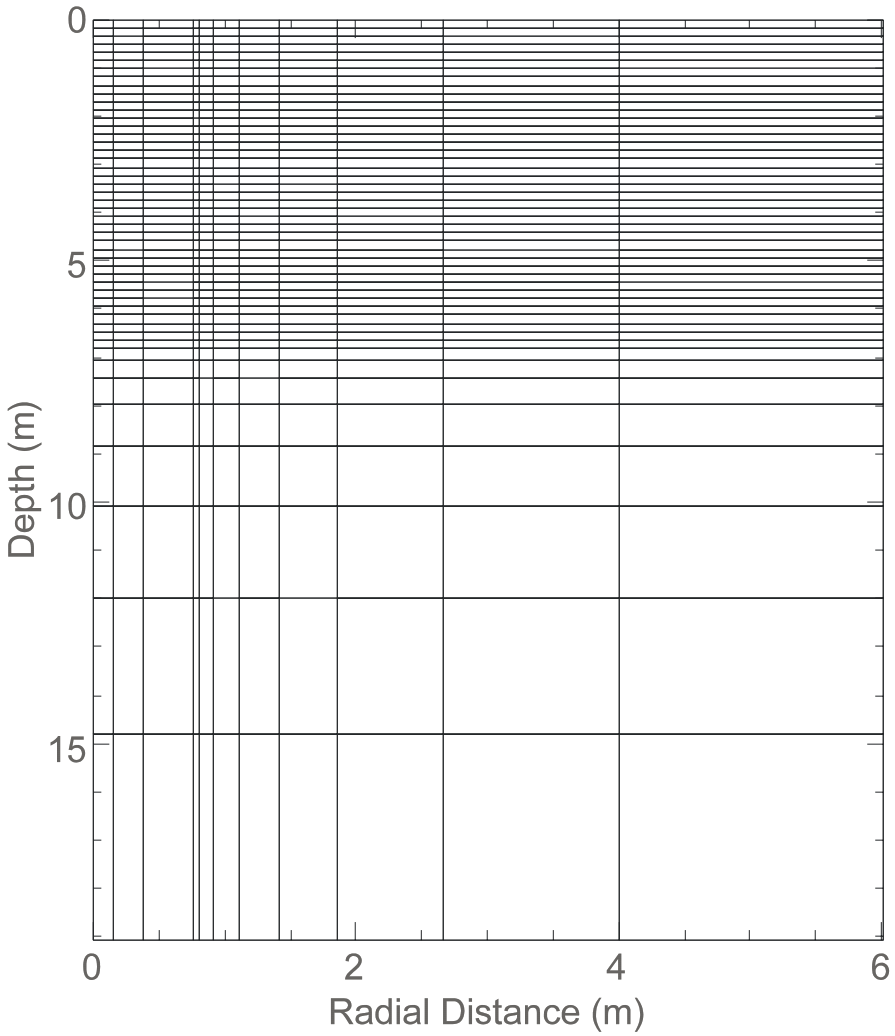

Figure 17. Spatial grid discretization used for the two-dimensional model.

5.2 Model Boundaries

The boundary conditions used in the 2-D model are consistent with the 1-D model. Atmospheric pressure and a diffusion boundary condition allowing for diffusion of HTO and $^{14}CO_2$ into the atmosphere are assigned at the domain top. The bottom boundary condition is constant pressure (Dirichlet boundary condition). Constant aqueous-phase pressure corresponding to initial 90% saturation is maintained. No-flow boundary condition is assigned on the inner and outer radial boundary.

5.3 Two-Dimensional Model Calibration

The 2-D model was calibrated with the contaminant concentrations from monitoring ports in the surface soil and the estimated HTO diffusion rates into the atmosphere. The tortuosity calculation in the soil layer above the beryllium blocks (described in the transport parameter estimation, Section 3.3.1) was calculated to be 9.45. Figure 18 shows the comparison of moisture content profiles of measured versus modeled; an agreement in the range of 0-20% moisture content was obtained. The HTO concentration in the aqueous phase in the soil at the GSP-1 ports, located at 2.7-, 4.5-, and 6.2-m depth and 0.3 m away from the outer radial surface of the auger hole in the model, was compared with the measured concentrations. The GSP-1 ports extracted the soil gas samples, which were then analyzed for contaminant concentrations. Olson et al. (2003) report the HTO concentration in the soil gas samples condensate. Prudic, Stonestrom, and Striegl (1997) report that the fractionation factor for ^{3}H between liquid water and water vapor varies from 1.108 to 1.103. Assuming an average fractionation factor of 1.0915, the HTO concentration in the soil aqueous phase was estimated based on the condensate concentration and then compared with the model-predicted soil moisture concentrations. The results are plotted in Figures 19, 20, and 21. The model overpredicted the HTO concentrations by one or two orders of magnitude. Similarly, the $^{14}CO_2$ monitoring data were reported as total activity and total gas sample volumes (Olson et al. 2003) from which the soil air-phase concentration of $^{14}CO_2$ was calculated. Thus, the $^{14}CO_2$ soil air-phase concentrations at the GSP-1 ports, located at 2.7-, 4.5-, and 6.2-m depth and 1 m away from the axis of the hole from the model, were compared with the measured concentrations. The results are plotted in Figures 22, 23, and 24. The differences in the concentrations were in the range of one to two orders of magnitude. The overprediction of $^{14}CO_2$ concentrations is conservative when estimating mass loss to atmosphere.

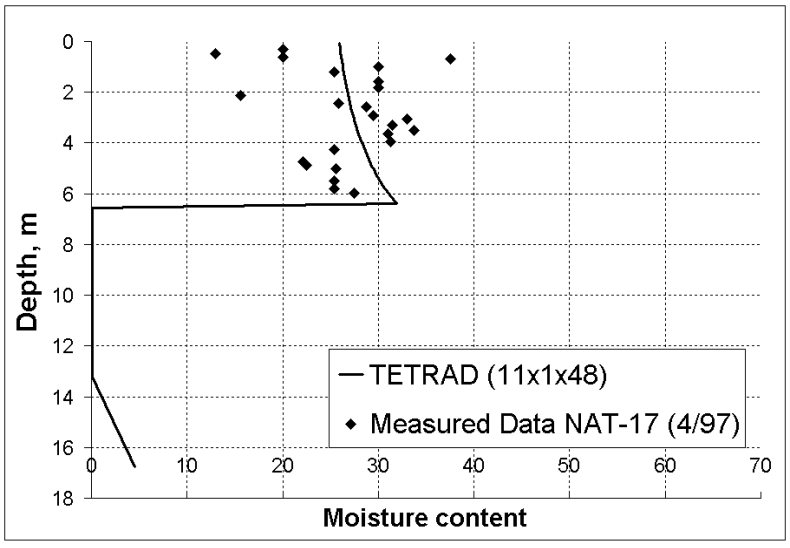

Figure 18. Comparison of measured moisture content profiles with steady-state model-predicted moisture content.

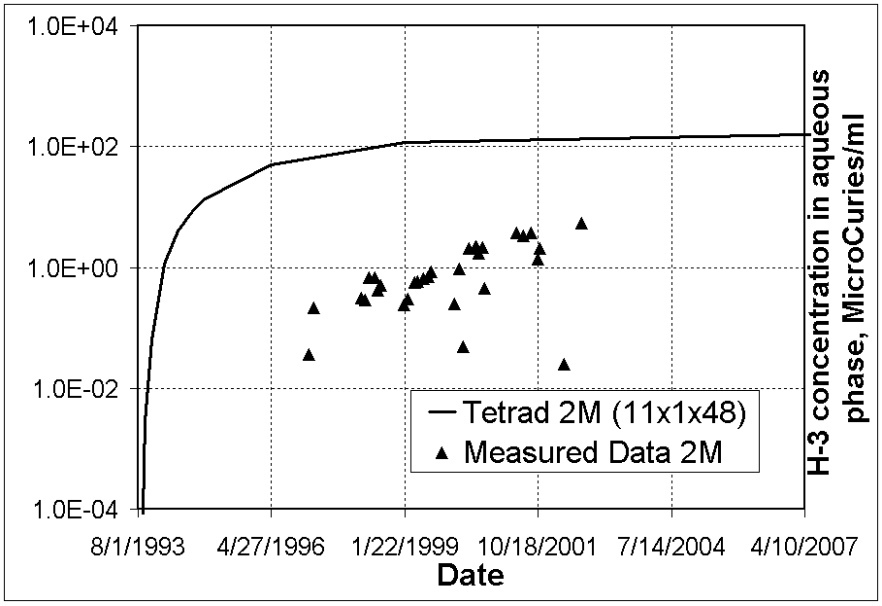

Figure 19. Tritiated water concentration in the soil aqueous phase measured by GSP-1 at the 2.7-m level.

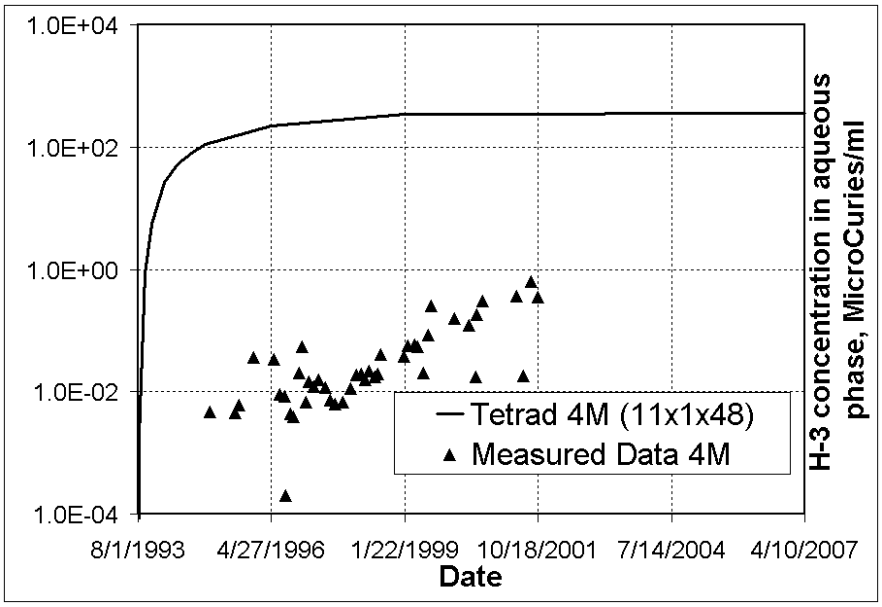

Figure 20. Tritiated water concentration in the soil aqueous phase measured by GSP-1 at the 4.5-m level.

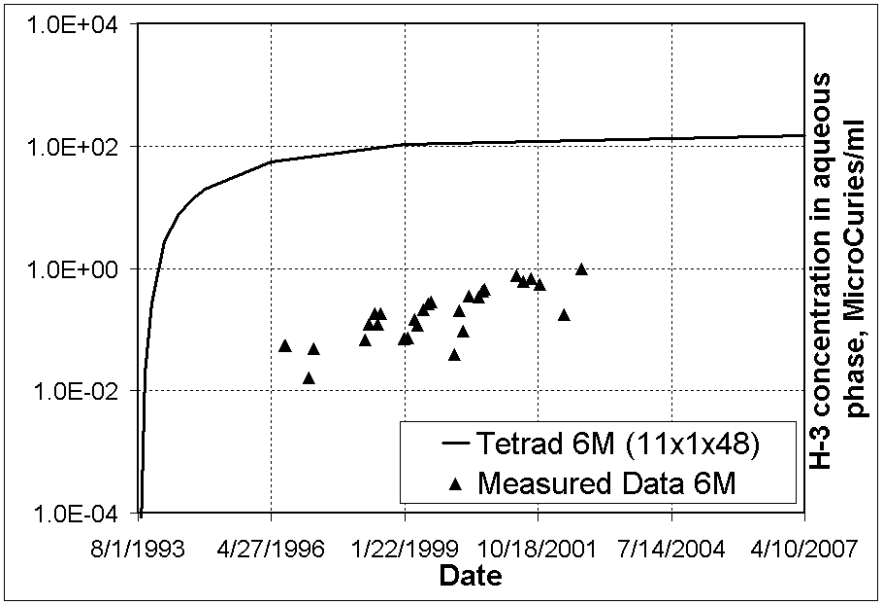

Figure 21. Tritiated water concentration in the soil aqueous phase measured by GSP-1 at the 6.2-m level.

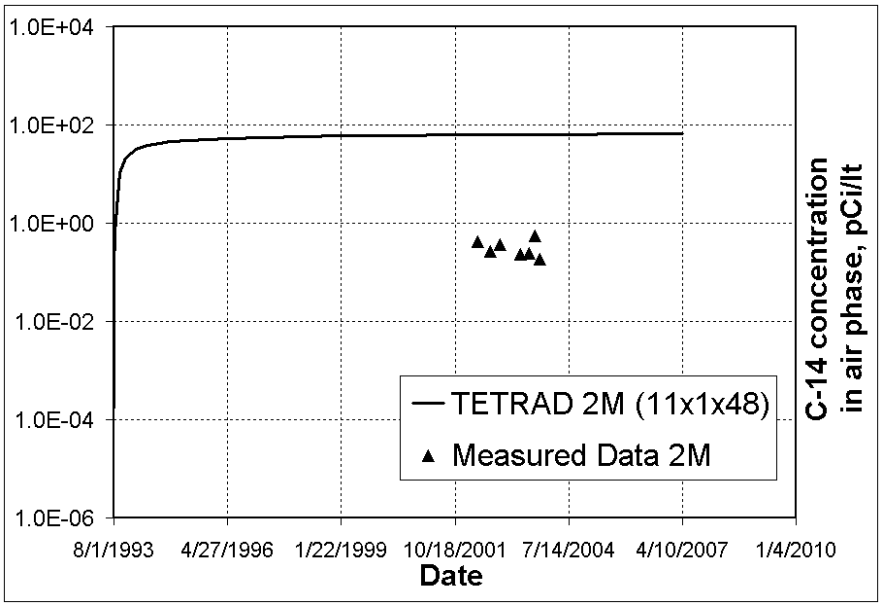

Figure 22. The $^{14}CO_2$ concentration in the soil air phase measured by GSP-1 at the 2.7-m level.

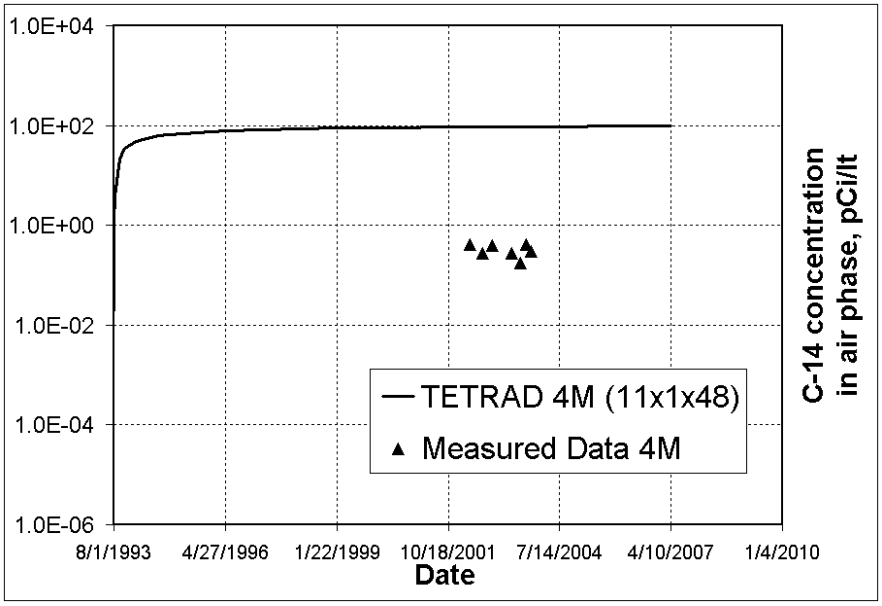

Figure 23. The $^{14}CO_2$ concentration in the soil air phase measured by GSP-1 at the 4.5-m level.

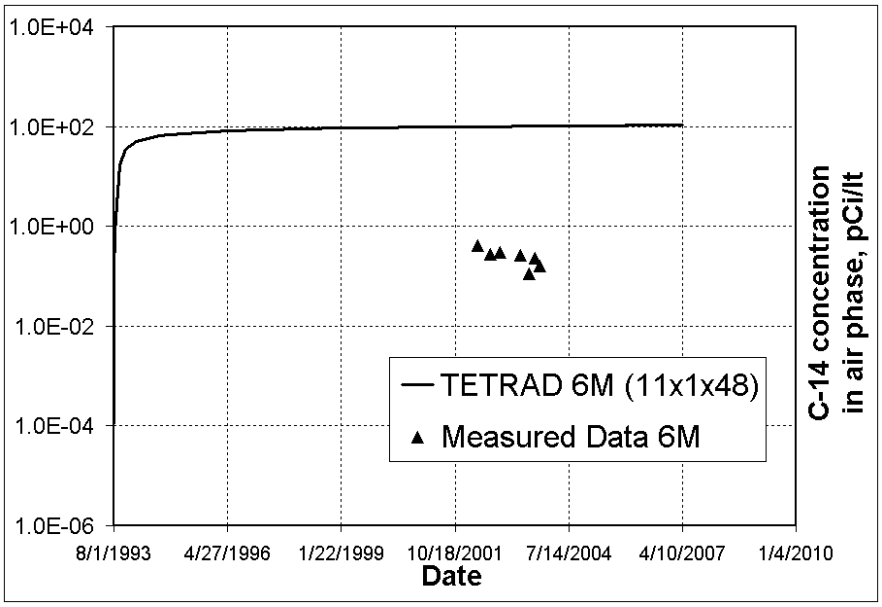

Figure 24. The $^{14}CO_2$ concentration in the soil air phase measured by GSP-1 at the 6.2-m level.

There was one more measurement port (i.e., IPV-5) located at 5.4-m depth and 5 m away from the axis of the auger hole. The model versus measured $^{14}CO_2$ concentration in the soil air phase is plotted in Figure 25, and an agreement in the range of one to two orders of magnitude was obtained. The estimated HTO diffusion rate to the atmosphere was compared with the model diffusion rates in Figure 26. The model diffusion rates were in reasonable agreement (i.e., within two orders of magnitude lower) with the estimated diffusion rates. For this calibrated model, the sensitivity study of the parameters was not conducted because the 1-D model was already calibrated through the sensitivity study, and the parameters that were used in the 1-D model were applied to the 2-D model.

5.4 Two-Dimensional Model Prediction

In this section, predictive results from the 2-D model for HTO and $^{14}CO_2$ concentrations, surface diffusion rates, material balance, and effective source release rates will be discussed. The concentrations of HTO at IPV-5 are obtained from the model and are discussed below. Upon obtaining additional monitoring data of HTO at IPV-5, comparisons could be performed with the modeled concentration history for further calibration. The amount of HTO and $^{14}CO_2$ migrating to the atmosphere from the model's total soil-atmosphere boundary surface and directly above the auger hole soil-atmosphere boundary surface is compared to understand the relative importance of vertical versus lateral migration. The material balance analysis of HTO and $^{14}CO_2$ was conducted to understand its relative distribution into the soil vapor and liquid, adsorption onto soil surface, and surface diffusion into the atmosphere at the top surface and advection at the bottom surface. The effective cumulative source release was calculated by subtracting the surface diffusional losses to the atmosphere from the original cumulative source release. An average effective source release rate was obtained from the effective cumulative source release amounts. A discussion of these results is given in the following paragraphs.

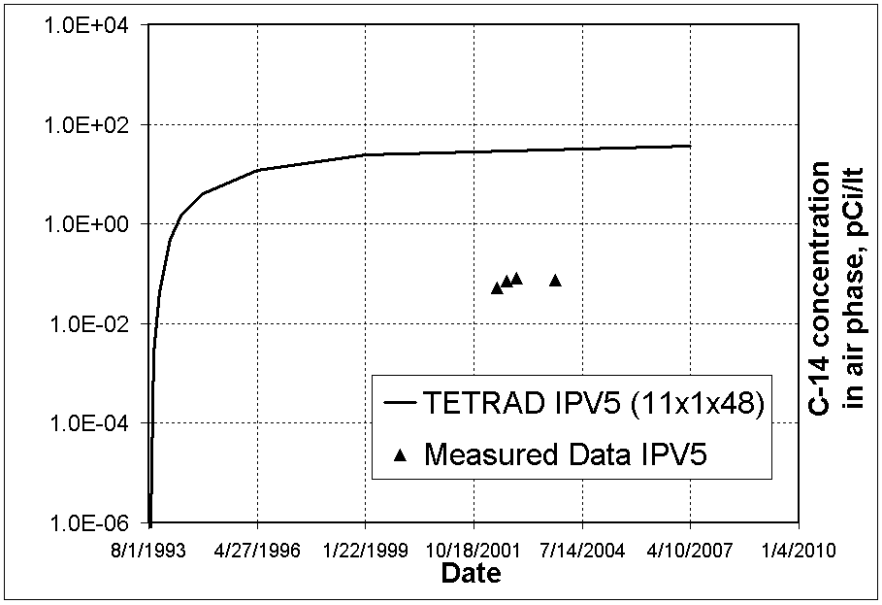

Figure 25. The $^{14}CO_2$ concentration in the soil air phase measured by IPV-5 at a 5-m distance away from the auger hole axis.

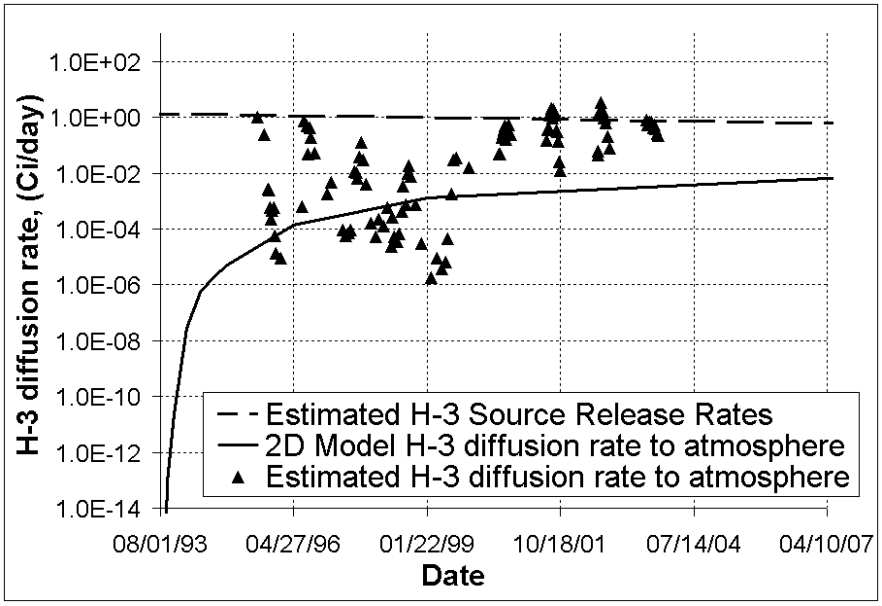

Figure 26. Comparison of two-dimensional model-predicted tritiated water diffusion rate to the atmosphere with the estimated diffusion rate to the atmosphere; also shown is the source release rate of tritiated water.

Profiles of HTO and $^{14}CO_2$ concentrations in the soil aqueous phase and soil vapor phase at 1-m distance radially away from the auger hole axis obtained from the 2-D model were plotted in Figure 27. Figure 28 shows the HTO soil aqueous phase concentration history at the IPV-5 measurement port, located 5 m away from the axis of the auger hole and at 5.4-m depth from the surface in the 2-D model. At IPV-5, the HTO soil aqueous-phase concentration at 01/1999 is 0.001 μCi/mL, while at 04/2000, the HTO soil aqueous-phase concentration is 0.073 μCi/mL. Compared to the 6.2-m GSP-1 modeled concentrations of 81.2 μCi/mL and 203 μCi/mL at 01/1999 and 04/2007, the IPV-5 HTO concentrations are three to five orders of magnitude lower. Because of slow diffusion in the lateral direction, the concentration at IPV-5 is lower than the GSP-1 port concentrations but is steadily increasing as more HTO migrates laterally.

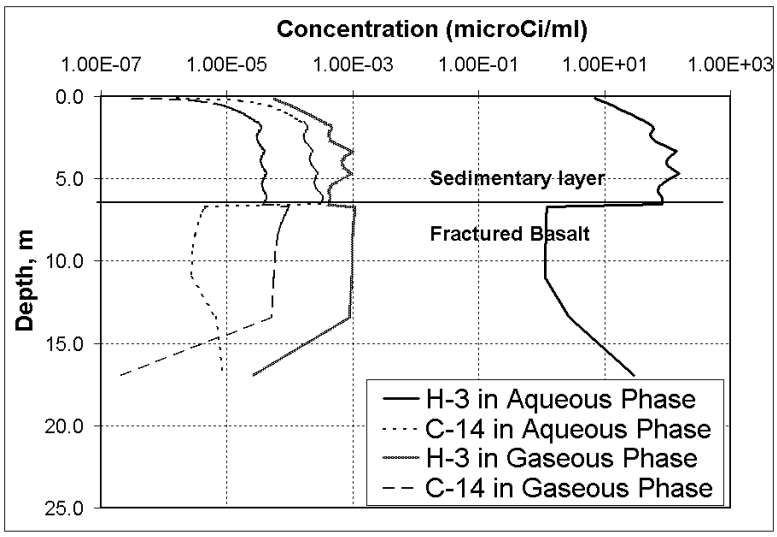

Figure 27. The profiles of tritiated water and $^{14}CO_2$ concentrations in the soil aqueous phase and soil vapor phase a 1-m distance radially away from the auger hole axis.

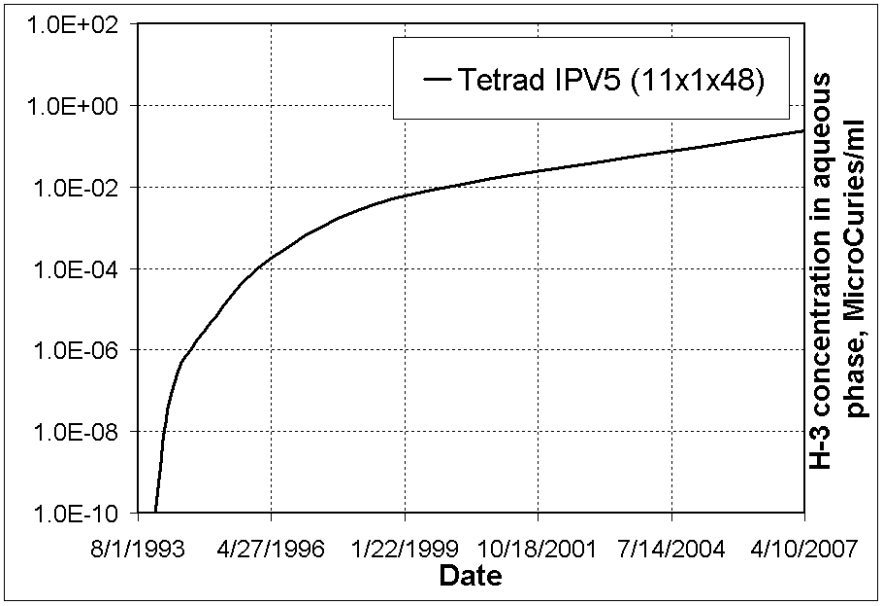

Figure 28. Tritiated water concentration in soil aqueous phase at IPV-5 (5 m away from the auger hole axis) obtained from the two-dimensional model.

The HTO and $^{14}CO_2$ diffusion rate into the atmosphere from the 1-D model and the 2-D model is compared with the source release rate in Figure 29 and Figure 30, respectively. The plots show that the total HTO diffusion rate in the 2-D model is 2.5 times higher than the 1-D model, while the $^{14}CO_2$ diffusion rates from the 2-D model are 1.25 times higher than the 1-D model. From the 2-D model, the cumulative amount of HTO and $^{14}CO_2$ diffusing into the atmosphere over the model's total soil-atmosphere boundary surface and directly above the auger hole soil-atmosphere boundary surface as a percentage of the cumulative source release is plotted in Figure 31 and Figure 32, respectively. Over a 22-year simulation period, 0.6% of cumulative source released HTO diffuses into the atmosphere from the total surface, and 0.12% diffuses out above the auger hole alone. For $^{14}CO_2$, over a 22-year simulation period, 81.7% of cumulative source released diffuses into the atmosphere from the total surface, and only 5.1% diffuses out above the auger hole surface. These results suggest that a major fraction of the released $^{14}CO_2$ is lost to the atmosphere by surface diffusion, while a major fraction of HTO is retained in the subsurface. Also, $^{14}CO_2$ migrates further in the lateral direction compared to HTO. For both the 1-D and 2-D models, the fraction of cumulative $^{14}CO_2$ diffusing to the atmosphere with respect to cumulative source released was approximately two to three orders of magnitude larger than the fractional cumulative diffusion amount of HTO to the atmosphere with respect to cumulative source released. This behavior could be attributed to the following reasons: the equilibrium ratios for HTO and $^{14}CO_2$ are 1.35E–2 and 3.42E+3 at 84.8 kPa and 10°C, respectively, implying HTO predominantly is present in the soil aqueous phase, and $^{14}CO_2$ is predominantly present in the soil vapor phase. The molecular diffusivity coefficients of HTO and $^{14}CO_2$ in the vapor phase are 2.22 m^2/day and 1.6 m^2/day. The HTO diffusivity coefficient is not markedly higher than the $^{14}CO_2$ diffusivity coefficient. Therefore, these reasons would intuitively suggest that the diffusion rate of $^{14}CO_2$ to the atmosphere at ground surface would be higher than the HTO diffusion rate. The simulation results show the same trend. The 2-D radial model is more accurate than the 1-D model because it allows for the migration of contaminants laterally into the vadose zone soil. Also, the lateral concentrations of both HTO and $^{14}CO_2$ were compared with the measured data, thus decreasing the uncertainty level of the model and making it a more realistic representation of SVR-20.

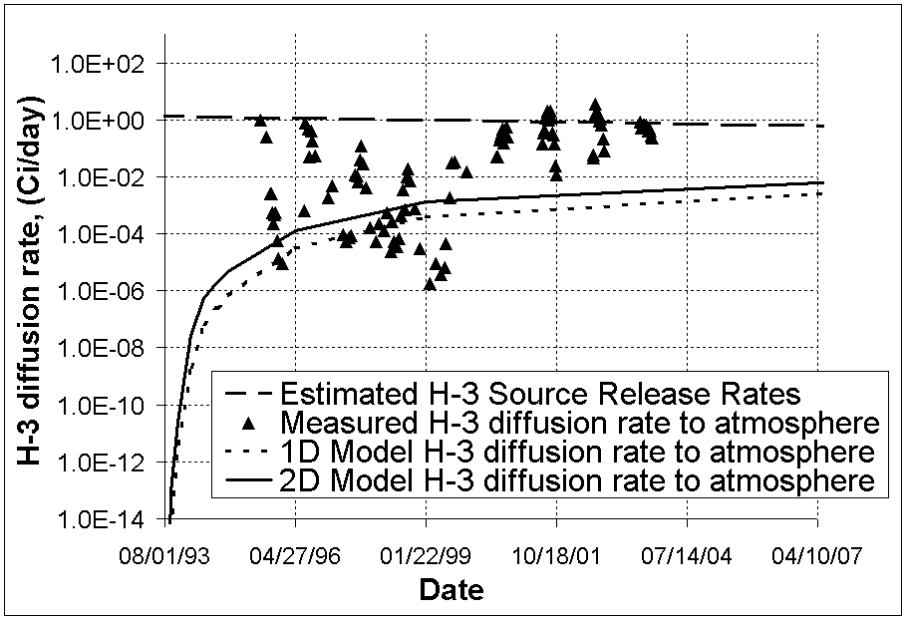

Figure 29. Model-predicted tritiated water surface diffusion rate to the atmosphere compared to the estimated surface diffusion rates to the atmosphere (based on measurements) and source release rates.

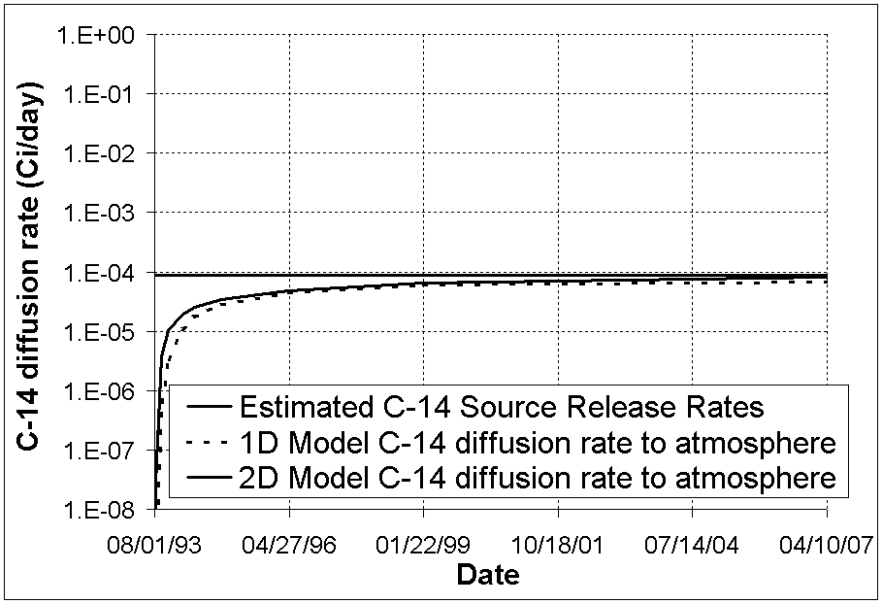

Figure 30. Model-predicted $^{14}CO_2$ surface diffusion rate to the atmosphere compared to the source release rates.

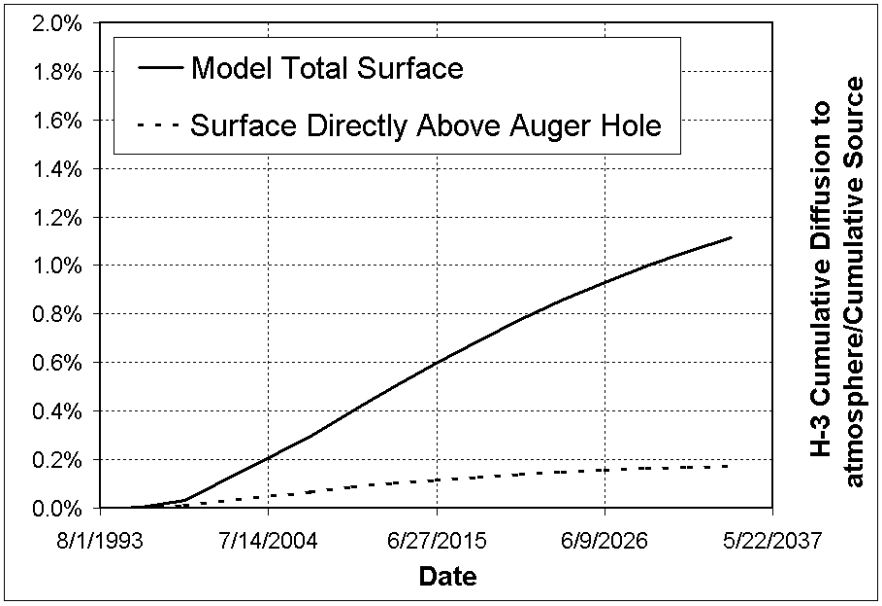

Figure 31. Comparison of fractional cumulative mass of tritiated water diffused to the atmosphere with respect to cumulative source released over the model's total soil-atmosphere boundary surface and directly above the auger hole surface.

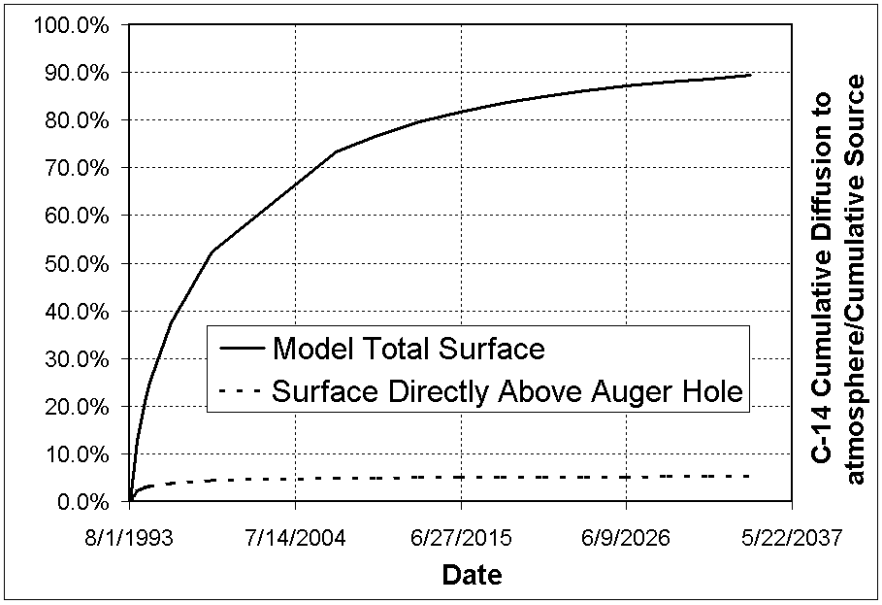

Figure 32. Comparison of fractional cumulative mass of $^{14}CO_2$ diffused to the atmosphere with respect to cumulative source release over the model's total soil-atmosphere boundary surface and directly above the auger hole atmosphere-soil boundary surface.

The mass balance of HTO and $^{14}CO_2$ showing distribution of the cumulative source released into the cumulative sink (diffusion at top and advection at bottom), adsorption, and storage in place is shown in Figure 33 and Figure 34, respectively. In Figure 35, a plot of the normalized cumulative mass balance error for H-3 and C-14 components is shown, a value of near zero (perfect material balance) is obtained for H-3, and approximately 2.0E–3 (acceptable) is obtained for C-14.

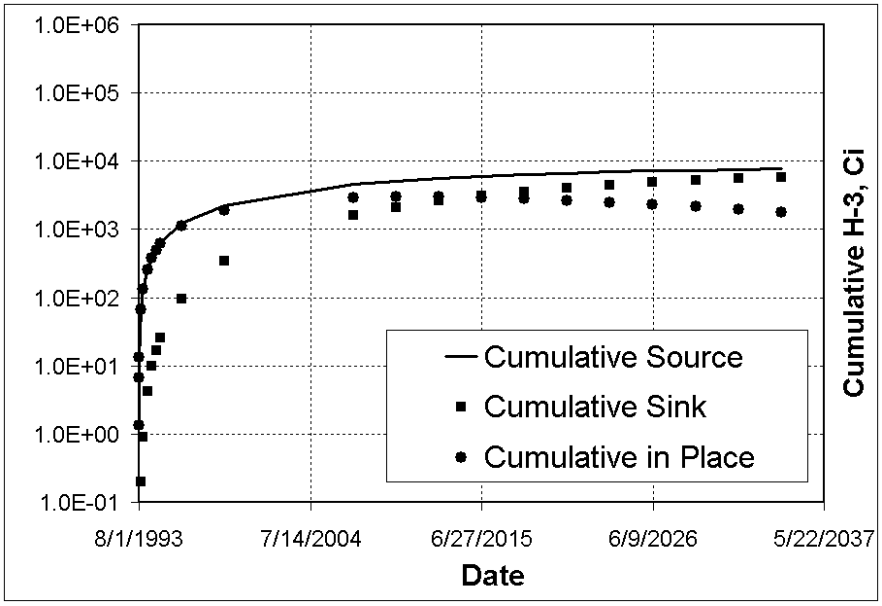

Figure 33. Mass balance of tritiated water showing the distribution of cumulative source into cumulative sink (diffusion at top and advection at bottom) and storage in place.

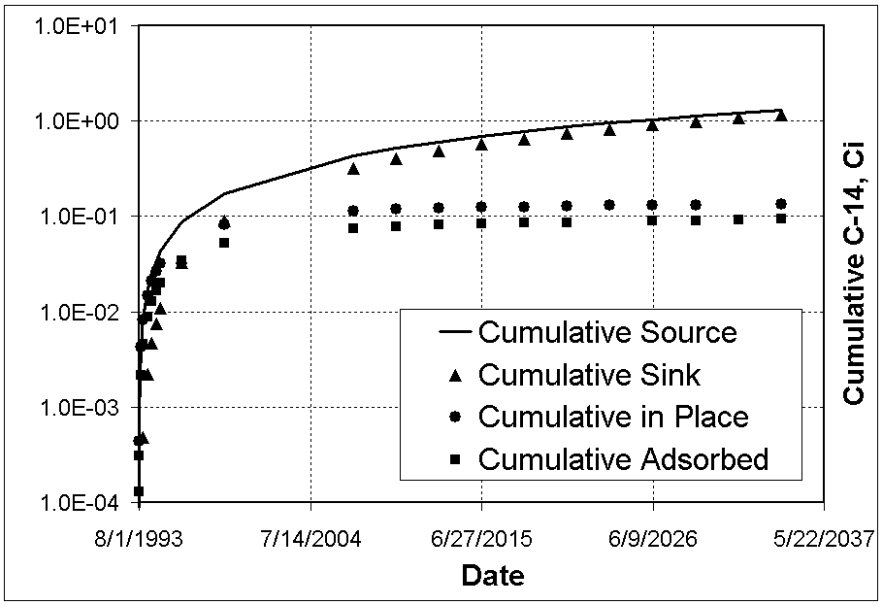

Figure 34. Mass balance of $^{14}CO_2$ showing the distribution of cumulative source into cumulative sink (diffusion at top and advection at bottom), adsorption onto soil, and storage in place.

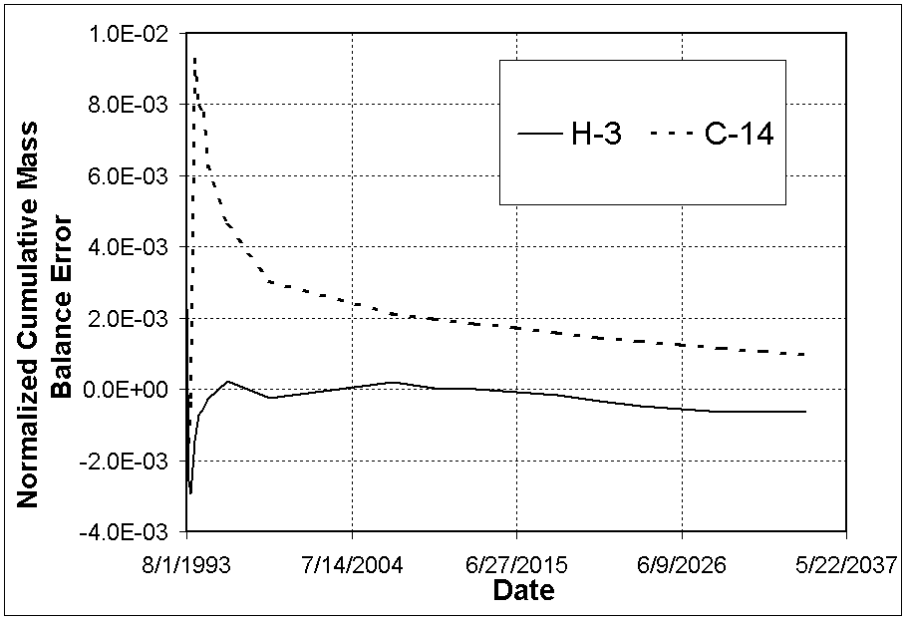

Figure 35. Plot of the normalized cumulative mass balance error for tritium and carbon-14.

The main goal of the project was to provide an effective source release rate of contaminants $^{14}CO_2$ and HTO into the subsurface for the field-scale model by taking into account the surface diffusion into the atmosphere. The effective cumulative source release rate and average effective source release rates were calculated and plotted in Figure 36 and Figure 37, respectively.

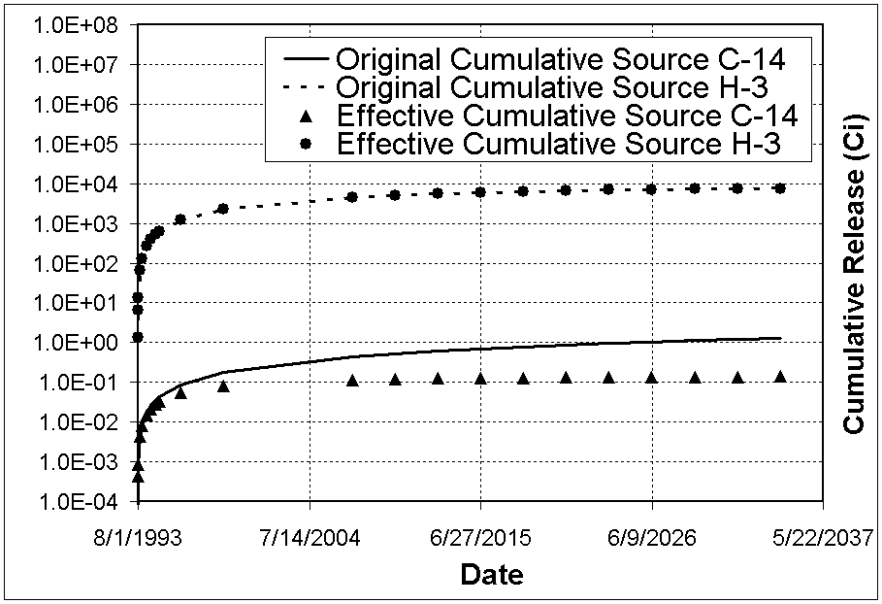

Figure 36. The cumulative original source release and effective (accounting for atmospheric diffusion) source release in Curies of tritiated water and $^{14}CO_2$.

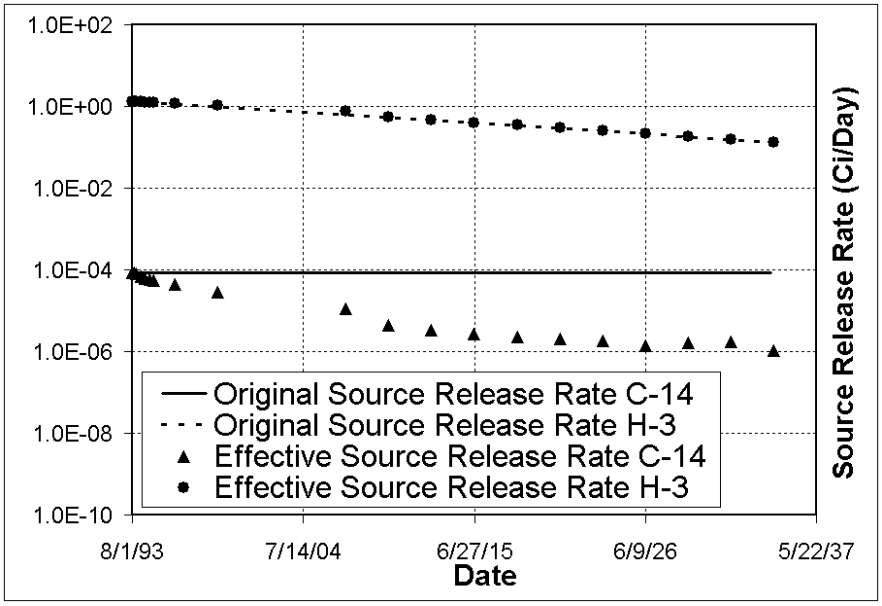

Figure 37. The original source release and effective (accounting for atmospheric diffusion) source release rate in Curies/day of tritiated water and $^{14}CO_2$.

6. MODEL LIMITATIONS

The model has the following limitations:

- Homogenous and isotropic porous media was assumed for the soil layer.
- A uniform inventory level was assigned to each of the beryllium blocks. In reality, depending on how long each of these beryllium blocks has been irradiated, each block can have its own different inventory levels, and there could be significant differences in the individual block inventory.
- The validity of the assumption of equal mass loading of HTO and ^{14}C within the blocks is uncertain since variability in the blocks exists. There could be different flux release rates at the openings between the baskets.
- The validity of uniform contaminant release rates at the openings is uncertain.
- Isothermal conditions in the model were assumed. In reality, seasonal temperatures vary in the top soil layer, which could have a significant effect on the diffusion rate. This effect was not incorporated into the model.

7. SUMMARY AND CONCLUSIONS

A summary of activities and findings from the numerical simulation study includes:

- 1-D and 2-D radial models for SVR-20 were developed using TETRAD.
- The 1-D model was calibrated with respect to the estimated diffusion rates into the atmosphere based on atmospheric concentration measurements above surface.
- Sensitivity analysis of the 1-D model was performed. The infiltration rate was found to have a major effect, while the barometric pumping effects and residual water saturation did not have significant effects on the ^{3}H diffusion rate out to the atmosphere at the surface.
- The 2-D model was calibrated with concentration measurements in the soil gas samples taken near the source (i.e., GSP-1 and IPV-5) and from the estimated diffusion rates into the atmosphere based on atmospheric concentration measurements above surface.
- In the 2-D model, the cumulative surface diffusion of $^{14}CO_2$ to the atmosphere accounts for 81.7% of the cumulative source released, and for HTO, the cumulative surface diffusion accounts for 0.6% of the cumulative source released over a 22-year simulation period. These results suggest that a major fraction of the released $^{14}CO_2$ is lost to the atmosphere by surface diffusion, while a major fraction of HTO is retained in the subsurface.

The overall conclusion is that the ^{14}C release rates from the beryllium blocks for the OU 7-13/14 full vadose zone model should be reduced by a time-variant factor to account for the near-field diffusion into atmosphere as given in Figures 36 and 37.

8. REFERENCES

Adler Flitton, M. Kay, Carolyn W. Bishop, Ronald E. Mizia, Lucinda L. Torres, and Robert D. Rogers, 2001, *Long Term Corrosion/Degradation Test Third-Year Results*, INEEL/EXT-01-00036, Rev. 0, Idaho National Engineering and Environmental Laboratory.

DOE-ID, 1991, *Federal Facility Agreement and Consent Order for the Idaho National Engineering Laboratory*, Administrative Docket No. 1088-06-29-120, U.S. Department of Energy Idaho Operations Office; U.S. Environmental Protection Agency, Region 10; and Idaho Department of Health and Welfare.

EDF-3394, 2004, "Simulation of Carbon-14 Transport in a Mesoscale Experiment," Idaho Completion Project.

EDF-4835, 2004, "Evaluation of Beryllium Corrosion Data and Tritium Modeling," Rev. 0, Idaho Completion Project.

Flickinger, Michael C. and Stephen W. Drew, 1999, *Encyclopedia of Bioprocess Technology: Fermentation, Biocatalysis, and Bioseparation*, Vol. 1–5, New York: John Wiley & Sons, Inc.

Holdren, K. Jean and Barbara J. Broomfield, 2003, *Second Revision to the Scope of Work for the Operable Unit 7-13/14 Waste Area Group 7 Comprehensive Remedial Investigation/Feasibility Study*, INEL-95/0253, Rev. 2, Idaho National Engineering and Environmental Laboratory.

Holdren, K. Jean, Bruce H. Becker, Nancy L. Hampton, L. Don Koeppen, Swen O. Magnuson, T. J. Meyer, Gail L. Olson, and A. Jeffrey Sondrup, 2002, *Ancillary Basis for Risk Analysis of the Subsurface Disposal Area,* INEEL/EXT-02-01125, Idaho National Engineering and Environmental Laboratory.

Hull, L. C. and F. A. Hohorst, 2001, *Transport Models for Radioactive Carbon Dioxide at RWMC*, INEEL/EXT-01-00894, Rev. 0, Idaho National Engineering and Environmental Laboratory.

Koeppen, L. Don, Alva M. Parsons, A. Jeffrey Sondrup, Paul D. Ritter, and Gail L. Olson, 2004, *Fiscal Year 2003 Environmental Monitoring Report for the Radioactive Waste Management Complex*, ICP/EXT-04-00259, Rev. 1, Idaho National Engineering and Environmental Laboratory.

Magnuson, S. O. and A. J. Sondrup, 1998, *Development, Calibration, and Predictive Results of a Simulator for Subsurface Pathway Fate and Transport of Aqueous- and Gaseous-Phase Contaminants in the Subsurface Disposal Area at the Idaho National Engineering and Environmental Laboratory*, INEEL/EXT-97-00609, Rev. 0, Idaho National Engineering and Environmental Laboratory.

Millington, R. J., 1959, "Gas Diffusion in Porous Media," *Science*, Vol. 130, pp. 100–102.

Mullen, Carlen K., Glen R. Longhurst, Michael L. Carboneau, and James W. Sterbentz, 2003, *Beryllium Waste Transuranic Inventory in the Subsurface Disposal Area, Operable Unit 7-13/14*, INEEL/EXT-01-01678, Rev. 2, Idaho National Engineering and Environmental Laboratory.

Olson, Gail L., L. Don Koeppen, Alva M. Parsons, Paul D. Ritter, and A. Jeffrey Sondrup, 2003, *FY 2002 Environmental Monitoring Report for the Radioactive Waste Management Complex*, INEEL/EXT-03-00055, Rev. 0, Idaho National Engineering and Environmental Laboratory.

Prudic, D. E., D. A. Stonestrom, and R. G. Striegl, 1997, *Tritium, Deuterium, and Oxygen-18 in Water Collected from Unsaturated Sediments Near a Low-Level Radioactive Waste Burial Site South of Beatty, Nevada*, 97-4062, United States Geological Survey.

Ritter, P. D., and D. L. McElroy, 1999, *Progress Report: Tritium and Carbon-14 Sampling at the Radioactive Waste Management Complex*, INEEL/EXT-98-00669, Rev. 1, Idaho National Engineering and Environmental Laboratory.

Rose, C. W., 1966, *Agricultural Physics*, New York: Elsevier Science.

Sandler, S. I., 1989, *Chemical and Engineering Thermodynamics*, New York: John Wiley & Sons.

Shook, G. M., 1995, *Development of an Environmental Simulator from Existing Petroleum Technology*, INEL-94/0283, Idaho National Engineering and Environmental Laboratory.

Smiles, D. E., W. R. Gardner, and R. K. Schulz, 1993, *Spherical Diffusion of Tritium from a Point of Release in a Uniform Unsaturated Soil*, NUREG/CR-6108, U.S. Nuclear Regulatory Commission.

Sposito, G., 1981, "Single Particle Motions in Liquid Water II. The Hydrodynamic Model," *Journal of Chemical Physics*, Vol. 74, pp. 6943–6949.

Vinsome, P. K. W. and G. M. Shook, 1993, "Multi-Purpose Simulation," *Journal of Petroleum Science and Engineering*, Vol. 9, pp. 29–38.

Appendix A

One-Dimensional Input Data File for Soil Vault Row 20

Appendix A
One-Dimensional Input Data File for Soil Vault Row 20

```
'NOMESS'
'COMMENT'  ' GOPI NALLA, 2004 '
'TYPE'    2  5  3  0.  0.
'UNITS'   1  1  0  0
'DIMEN'   1  1  48  100000
'PRINT'   0  1  0  0  0
'OUTFUN'  4  2  0  0  1  1  0  0  0  1
'OUTGEO'  0  2  0  0  0  0  0  0  0  0
'OUTPROP' 0  1  1  0  0  0  0  0  0  0
'OUTMISC' 8  1  0  1  1  0  1  0  0  1
'EXMBAL'  1
'NEWT'    15  1.0e-7  0.0  1.0
'SHIFT'  1.E-5,,,,,,,,,
'DELX' 1
 1       1.33
'DELY'  1
1        1.33
'DELZ'  10
 39     39*0.166
 1       0.166
 1       0.249
 1       0.3735
 1       0.5602
 1       0.8404
 1       1.2605
 1       1.8908
 1       2.8363
 1       4.2544

'FTOPS'   0 0
'PORMOD'      1    12     1   0.50  'top sediment GWS'
'PORMOD'      13   35     1   0.95  'voids around blocks'
'PORMOD'      36   39     1   0.50  'bottom sediment GWS'
'PORMOD'      40   48     1   0.05  'frac basalt'
'COMMENT' ' '
'PERMMOD'     1    12     1   680.0  680.0  680.0
'PERMMOD'     13   35     1   100.0  100.0  100.0
'PERMMOD'     36   39     1   680.0  680.0  680.0
'PERMMOD'     40   48     1   9000.0  9000.0  300.0
'PROPERTY'
'SATMOD'      1   12   1   0.100  0.00
'SATMOD'      13  35   1   0.999  0.00
'SATMOD'      36  39   1   0.100  0.00
'SATMOD'      40  48   1   0.100  0.00
'TEMPMOD'     1   48   1   10.
'DENRMOD'     1   48   1   2700.
'WMOD'        1   48  1   1.  0.  0.  0.  0.
'YMOD'        1   48  1   0.  0.  0.  1.  0.
'PRES'       84.8   0.0   0.0104
'VANGEN'  99  1  1.066  1.523  0.0  0.292  0.0  0.05  1.0  0.0  1.0,,,
'RELANAL' 99  3  0  1.
25.  25.  1.  0.  1.  0.
```

```
.0001   1.   2.00
0.   0.   1.1   32.  1.5
.01  1.  1.2
0.  0.  1.1    0.  1.
'RKREG'    1    12    1   1
'RKREG'    13   35    1   3
'RKREG'    36   39    1   1
'RKREG'    40   48    1   3
'DENCS'  1000. 1000. 1000.  1.22  1584.
         1  1  1   2  1
         18.02 18.02 18.02  29. 154.
'LIQDEN'
 1000.03 ,,,,,
 1000.03 ,,,,,,
 1000.03 ,,,,,,
 300.,,,,,,
 1584.,,,,,,
'CRITG'
 ,,,,,,,,
 ,,,,,,,,
 ,,,,,,,,
 3771.8  132.8  .0032
 5000.   550.  .0018
'LIQVIS'
 1. ,,,,,
 1. ,,,,,
 1. ,,,,,
 0.5  0.
 1.  0.
'GASVIS'
 .0181 0.  1.  0.  1.
 .0181 0.  1.  0.  1.
 .0181 0.  1.  0.  1.
 .0181 0.  1.  0.  1.
 .0181 0.  1.  0.  1.
'KVAL'  0.0 0.0  0.0   0.001  9.7e-5
1.186219e7  -2.095847e1  2.548592e-3  3816.44  46.130
1.186219e7  -2.095847e1  2.548592e-3  3816.44  46.130
2.9E+4    0.  0.  0.  0.
8.6212E8  0.  0.  3103.4  0.16
9.7   0.  0.  0.  0.
'RECUR'
'TIMEYR'  0
'TIME'    -100000.0  0.00001
'AQUIFER' 'SSTATE'  1  1  1  3  2  4  ,  ,  ,  ,  84.8  ,  ,  ,
,,,,,,,

'AQUIFER' 'SSTATE'  48  48  1  3  1   ,,,,,,,,,,,,,,,,

'MFLUX' 1 1 1  3  0.02738 0.  0. 0. 0.   '1.0 cm/yr'

'GVWRITE' -1  0
4 'PW' 'PG' 'SW' 'MFZ1'
'TIME'    -99990.    -1
'TIME'    -99000.   -1
'TIME'    -90000.   -1
'TIME'    -80000.   -1
```

```
'TIME'    -70000.   -1
'TIME'    -60000.   -1
'TIME'    -50000.   -1
'TIME'    -40000.   -1
'TIME'    -30000.   -1
'TIME'    -20000.   -1
'TIME'    -10000.   -1
'TIME'     -5000.   -1
'TIME'         0. .001
'GVWRITE' -1  0
8  'PW' 'PG' 'SW' 'SG' 'W2' 'MFZ1' 'MFZ2'  'MFZ3'
'COMMENT'  'radioactive decay'
'SCRACK'     2      1     1.0  ,,,
     0.0  5.635e-02 0.0    0.0    0.0    0.0   ,,,,,,,
'SCRACK'     3      1     1.0  ,,,
     0.0  1.210e-4  0.0    0.0    0.0    0.0   ,,,,,,,
'MOLDIFF'  -1. ,,,,,,,,,,
 0.      19.53e-5  4.32e-5   0.  0.
 0.      2.22    1.6   0.  0.
 0.      0.     0.   0.  0.
'DIFFBC' 1 1 1 3 2,,,,,,,,,,,,

'ADSORP'   1   1   ,,,,,,,,
0.     0.    1.
0.     0.    1.
0.8    0.    1.
0.     0.    1.
0.     0.    1.

'ADSREG'  1  48  1   1

'COMMENT'
'MFLUXT'        1       289
0.00        0.0     2.672E-09       3.79187E-10     0.0     0.0
365.20      0.0     2.526E-09       3.7913E-10      0.0     0.0
730.50      0.0     2.389E-09       3.79074E-10     0.0     0.0
1095.70     0.0     2.260E-09       3.79017E-10     0.0     0.0
1461.00     0.0     2.136E-09       3.79017E-10     0.0     0.0
1826.20     0.0     2.020E-09       3.78961E-10     0.0     0.0
2191.50     0.0     1.911E-09       3.78904E-10     0.0     0.0
2556.70     0.0     1.807E-09       3.78904E-10     0.0     0.0
2922.00     0.0     1.709E-09       3.78847E-10     0.0     0.0
3287.20     0.0     1.616E-09       3.78791E-10     0.0     0.0
3652.50     0.0     1.528E-09       3.78734E-10     0.0     0.0
4017.70     0.0     1.445E-09       3.78678E-10     0.0     0.0
4383.00     0.0     1.366E-09       3.78621E-10     0.0     0.0
4748.20     0.0     1.292E-09       3.78564E-10     0.0     0.0
5113.50     0.0     1.222E-09       3.78564E-10     0.0     0.0
5478.70     0.0     1.156E-09       3.78508E-10     0.0     0.0
5844.00     0.0     1.092E-09       3.78451E-10     0.0     0.0
6209.20     0.0     1.033E-09       3.78395E-10     0.0     0.0
6574.50     0.0     9.768E-10       3.78338E-10     0.0     0.0
6939.70     0.0     9.236E-10       3.78282E-10     0.0     0.0
7305.00     0.0     8.738E-10       3.78225E-10     0.0     0.0
7670.20     0.0     8.263E-10       3.78225E-10     0.0     0.0
8035.50     0.0     7.816E-10       3.78168E-10     0.0     0.0
8400.70     0.0     7.386E-10       3.78112E-10     0.0     0.0
```

```
8766.00     0.0     6.984E-10       3.78055E-10     0.0     0.0
9131.20     0.0     6.605E-10       3.78055E-10     0.0     0.0
9496.50     0.0     6.242E-10       3.77999E-10     0.0     0.0
9861.70     0.0     5.909E-10       3.77942E-10     0.0     0.0
10227.00    0.0     5.588E-10       3.77942E-10     0.0     0.0
10592.20    0.0     5.282E-10       3.77885E-10     0.0     0.0
10957.50    0.0     4.995E-10       3.77829E-10     0.0     0.0
11322.70    0.0     4.724E-10       3.77772E-10     0.0     0.0
11688.00    0.0     4.466E-10       3.77716E-10     0.0     0.0
12053.20    0.0     4.224E-10       3.77659E-10     0.0     0.0
12418.50    0.0     3.994E-10       3.77602E-10     0.0     0.0
12783.70    0.0     3.777E-10       3.77602E-10     0.0     0.0
13149.00    0.0     3.572E-10       3.77546E-10     0.0     0.0
13514.20    0.0     3.378E-10       3.77489E-10     0.0     0.0
13879.50    0.0     3.194E-10       3.77433E-10     0.0     0.0
14244.70    0.0     3.020E-10       3.77376E-10     0.0     0.0
14610.00    0.0     2.856E-10       3.77319E-10     0.0     0.0
14975.20    0.0     2.701E-10       3.77263E-10     0.0     0.0
15340.50    0.0     2.554E-10       3.77263E-10     0.0     0.0

'MFREG'   13  35  1   1

'TIME'      1.   -1
'TIME'      5.   -1
'TIME'     10.   -1
'TIME'     50.   -1
'TIME'    100.   -1
'TIME'    200.   -1
'TIME'    300.   -1
'TIME'    400.   -1
'TIME'    500.   -1
'TIME'   1000.   -1
'TIME'   2000.   -1
'TIME'   5000.   -1
'TIME'   6000.   -1
'TIME'   7000.   -1
'TIME'   8000.   -1
'TIME'   9000.   -1
'TIME'  10000.   -1
'TIME'  11000.   -1
'TIME'  12000.   -1
'TIME'  13000.   -1
'TIME'  14000.   -1
'TIME'  15000.    0.
```

Appendix B

Two-Dimensional Input Data File for Soil Vault Row 20

Appendix B
Two-Dimensional Input Data File for Soil Vault Row 20

```
'NOMESS'
'COMMENT'  'GOPI NALLA, 2004 '
'TYPE'    2  5  3  0.  0.
'UNITS'   1  1  0  0
'DIMEN'   11 1 48 100000
'PRINT'   0  1  0  0  0
'OUTFUN'  4  2  0  0  1  1  0  0  0  1
'OUTGEO'  0  2  0  0  0  0  0  0  0  0
'OUTPROP' 0  1  1  0  0  0  0  0  0  0
'OUTMISC' 8  1  0  1  1  0  1  0  0  3
'EXMBAL'  1
'NEWT'    15   1.0e-7  0.0  1.0
'SHIFT'  1.E-5,,,,,,,,,
'DELX' 11
 1      0.15
 1      0.225
 1      0.375
 1      0.05
 1      0.10
 1      0.20
 1      0.30
 1      0.45
 1      0.80
 1      1.35
 1      2.00
'DELZ'  10
 39     39*0.166
 1       0.166
 1       0.249
 1       0.3735
 1       0.5602
 1       0.8404
 1       1.2605
 1       1.8908
 1       2.8363
 1       4.2544
'RADIAL' 0  0.0
'FTOPS'   0 0
'PORMOD'      1    319     1   0.50
'PORMOD'      320  429     1   0.50
'PORMOD'      430  528     1   0.05
'PORMOD'      133  209     11  0.95
'PORMOD'      221  297     11  0.95
'PORMOD'      309  385     11  0.95
'PORMOD'      134  209     11  0.95
'PORMOD'      222  297     11  0.95
'PORMOD'      310  385     11  0.95
'PORMOD'      135  209     11  0.95
'PORMOD'      223  297     11  0.95
'PORMOD'      311  385     11  0.95
'PORMOD'      136  209     11  0.00
'PORMOD'      224  297     11  0.00
```

```
'PORMOD'      312  385     11  0.00
'PERMMOD'     1    319     1   680.0  680.0  680.0
'PERMMOD'     320  429     1   680.0  680.0  680.0
'PERMMOD'     430  528     1   9000.0  9000.0  300.0
'PERMMOD'     133  209    11   100.0 100.0 100.0
'PERMMOD'     221  297    11   100.0 100.0 100.0
'PERMMOD'     309  385    11   100.0 100.0 100.0
'PERMMOD'     134  209    11   100.0 100.0 100.0
'PERMMOD'     222  297    11   100.0 100.0 100.0
'PERMMOD'     310  385    11   100.0 100.0 100.0
'PERMMOD'     135  209    11   100.0 100.0 100.0
'PERMMOD'     223  297    11   100.0 100.0 100.0
'PERMMOD'     311  385    11   100.0 100.0 100.0
'PERMMOD'     136  209    11     0.0   0.0   0.0
'PERMMOD'     224  297    11     0.0   0.0   0.0
'PERMMOD'     312  385    11     0.0   0.0   0.0
'PROPERTY'
'SATMOD'      1   528   1   0.100  0.00
'SATMOD'     133  209   11  0.99  0.00
'SATMOD'     221  297   11  0.99  0.00
'SATMOD'     309  385   11  0.99  0.00
'SATMOD'     134  209   11  0.99  0.00
'SATMOD'     222  297   11  0.99  0.00
'SATMOD'     310  385   11  0.99  0.00
'SATMOD'     135  209   11  0.99  0.00
'SATMOD'     223  297   11  0.99  0.00
'SATMOD'     311  385   11  0.99  0.00
'SATMOD'     136  209   11  0.00  0.00
'SATMOD'     224  297   11  0.00  0.00
'SATMOD'     312  385   11  0.00  0.00
'TEMPMOD'     1   528   1   10
'DENRMOD'     1   528   1   2700.
'WMOD'        1   528  1   1.  0.  0.   0.  0.
'YMOD'        1   528  1   0.  0.  0.   1.  0.
'PRES'       84.8   0.0   0.0104
'VANGEN' 99  1  1.066  1.523  0.0  0.292  0.0  0.05  1.0  0.0  1.0,,,
'RELANAL' 99  3  0  1.
25.  25.  1.  0.  1.  0.
.0001   1.     2.00
0.   0.   1.1   32.  1.5
.01  1.  1.2
0.  0.  1.1    0.  1.
'RKREG'    1    319    1   1
'RKREG'    320  429    1   1
'RKREG'    430  528    1   3
'RKREG'    133  209   11   3
'RKREG'    221  297   11   3
'RKREG'    309  385   11   3
'RKREG'    134  209   11   3
'RKREG'    222  297   11   3
'RKREG'    310  385   11   3
'RKREG'    135  209   11   3
'RKREG'    223  297   11   3
'RKREG'    311  385   11   3
'RKREG'    136  209   11   3
'RKREG'    224  297   11   3
'RKREG'    312  385   11   3
```

```
'DENCS'  1000. 1000. 1000. 1.22  1584.
         1  1  1  2  1
         18.02 18.02 18.02 29. 154.
'LIQDEN'
 1000.03 ,,,,,
 1000.03 ,,,,,
 1000.03 ,,,,,,
 300.,,,,,,
 1584.,,,,,,
'CRITG'
 ,,,,,,,,
 ,,,,,,,,
 ,,,,,,,,
 3771.8  132.8  .0032
 5000.   550.  .0018
'LIQVIS'
1.  ,,,,,
1.  ,,,,,
1.  ,,,,,
 0.5  0.
 1.  0.
'GASVIS'
 .0181 0.  1.  0.  1.
 .0181 0.  1.  0.  1.
 .0181 0.  1.  0.  1.
 .0181 0.  1.  0.  1.
 .0181 0.  1.  0.  1.
'KVAL'  0.0 0.0 0.0     0.001  9.7e-5
1.186219e7  -2.095847e1  2.548592e-3  3816.44  46.130
1.186219e7  -2.095847e1  2.548592e-3  3816.44  46.130
2.9E+4    0.  0.  0.  0.
8.6212E8  0.  0.  3103.4  0.16
9.7   0.  0.  0.  0.
'DISPER'   0. 0. 0. 0. 0. 0.
'RECUR'
'TIMEYR'  0
'TIME'    -100000.0  0.00001
'AQUIFER' 'SSTATE' 1 11 1 3 2 4 , , , , 84.8 , , ,
,,,,,,,
'AQUIFER' 'SSTATE' 518  528  1   3    1   ,  ,  ,  ,  ,  ,  ,  ,
'MFLUX'  1  11   1  3   0.02738          0.    0.    0.    0.  '1.0 cm/yr'
'GVWRITE' -1  0
10  'PW' 'PG' 'SW'  'W2'  'W3'  'Y2'  'Y3'  'MFZ1'  'MFZ2'  'MFZ3'
'TIME'      -99990.     -1
'TIME'      -99000.     -1
'TIME'      -90000.     -1
'TIME'      -80000.     -1
'TIME'      -70000.     -1
'TIME'      -60000.     -1
'TIME'      -50000.     -1
'TIME'      -40000.     -1
'TIME'      -30000.     -1
'TIME'      -20000.     -1
'TIME'      -10000.     -1
'TIME'      -5000.      -1
'TIME'      -0.0001     -1
'TIME'       0.     .00001
```

```
'COMMENT'  'radioactive decay'
'SCRACK'     2      1     1.0  ,,,
    0.0  5.635e-02 0.0    0.0    0.0    0.0
'SCRACK'     3      1     1.0  ,,,
    0.0  1.210e-04 0.0    0.0    0.0    0.0
'MOLDIFF'  -1. ,,,,,,,,,,
0.   19.53e-5    4.32e-5    0.    0.
0.     2.22      1.6      0.0   0.0
0.       0.       0.       0.    0.
'DIFFBC'   1    11    1   3    2   ,,,,,,,,,,,,,,
'ADSORP'   1   1   ,,,,,,,,
0.     0.    1.
0.     0.    1.
0.8    0.    1.
0.     0.    1.
0.     0.    1.
'ADSREG'  1 528 1  1

'MFLUXT'    1     42
0.00        0.0   3.693E-09   5.23948E-10 0.0   0.0
365.20      0.0   3.491E-09   5.2387E-10  0.0   0.0
730.50      0.0   3.302E-09   5.23792E-10 0.0   0.0
1095.70     0.0   3.123E-09   5.23714E-10 0.0   0.0
1461.00     0.0   2.952E-09   5.23714E-10 0.0   0.0
1826.20     0.0   2.792E-09   5.23635E-10 0.0   0.0
2191.50     0.0   2.640E-09   5.23557E-10 0.0   0.0
2556.70     0.0   2.496E-09   5.23557E-10 0.0   0.0
2922.00     0.0   2.361E-09   5.23479E-10 0.0   0.0
3287.20     0.0   2.233E-09   5.23401E-10 0.0   0.0
3652.50     0.0   2.111E-09   5.23323E-10 0.0   0.0
4017.70     0.0   1.996E-09   5.23244E-10 0.0   0.0
4383.00     0.0   1.888E-09   5.23166E-10 0.0   0.0
4748.20     0.0   1.785E-09   5.23088E-10 0.0   0.0
5113.50     0.0   1.688E-09   5.23088E-10 0.0   0.0
5478.70     0.0   1.597E-09   5.2301E-10  0.0   0.0
5844.00     0.0   1.509E-09   5.22932E-10 0.0   0.0
6209.20     0.0   1.428E-09   5.22853E-10 0.0   0.0
6574.50     0.0   1.350E-09   5.22775E-10 0.0   0.0
6939.70     0.0   1.276E-09   5.22697E-10 0.0   0.0
7305.00     0.0   1.207E-09   5.22619E-10 0.0   0.0
7670.20     0.0   1.142E-09   5.22619E-10 0.0   0.0
8035.50     0.0   1.080E-09   5.2254E-10  0.0   0.0
8400.70     0.0   1.021E-09   5.22462E-10 0.0   0.0
8766.00     0.0   9.650E-10   5.22384E-10 0.0   0.0
9131.20     0.0   9.126E-10   5.22384E-10 0.0   0.0
9496.50     0.0   8.626E-10   5.22306E-10 0.0   0.0
9861.70     0.0   8.164E-10   5.22228E-10 0.0   0.0
10227.00    0.0   7.722E-10   5.22228E-10 0.0   0.0
10592.20    0.0   7.299E-10   5.22149E-10 0.0   0.0
10957.50    0.0   6.902E-10   5.22071E-10 0.0   0.0
11322.70    0.0   6.527E-10   5.21993E-10 0.0   0.0
11688.00    0.0   6.172E-10   5.21915E-10 0.0   0.0
12053.20    0.0   5.836E-10   5.21837E-10 0.0   0.0
12418.50    0.0   5.519E-10   5.21758E-10 0.0   0.0
12783.70    0.0   5.219E-10   5.21758E-10 0.0   0.0
13149.00    0.0   4.935E-10   5.2168E-10  0.0   0.0
13514.20    0.0   4.667E-10   5.21602E-10 0.0   0.0
```

```
13879.50    0.0   4.414E-10   5.21524E-10 0.0   0.0
14244.70    0.0   4.174E-10   5.21446E-10 0.0   0.0
14610.00    0.0   3.947E-10   5.21367E-10 0.0   0.0
14975.20    0.0   3.733E-10   5.21289E-10 0.0   0.0


'MFREG'           133   209   11    1
'MFREG'           134   209   11    1
'MFREG'           135   209   11    1
'MFREG'           221   297   11    1
'MFREG'           222   297   11    1
'MFREG'           223   297   11    1
'MFREG'           309   385   11    1
'MFREG'           310   385   11    1
'MFREG'           311   385   11    1

'TIME'      1.   -1
'TIME'      5.   -1
'TIME'     10.   -1
'TIME'     50.   -1
'TIME'    100.   -1
'TIME'    200.   -1
'TIME'    300.   -1
'TIME'    400.   -1
'TIME'    500.   -1
'TIME'   1000.   -1
'TIME'   2000.   -1
'TIME'   5000.   -1
'TIME'   6000.   -1
'TIME'   7000.   -1
'TIME'   8000.   -1
'TIME'   9000.   -1
'TIME'  10000.   -1
'TIME'  11000.   -1
'TIME'  12000.   -1
'TIME'  13000.   -1
'TIME'  14000.   -1
'TIME'  15000.    0.
```